Sacubitril/valsartan Inhibits Obesity-associated Diastolic Dysfunction through Suppression of Ventricular-vascular Stiffness

Annayya R Aroor
University of Missouri
Srinivas Mummidi
University of Texas Rio Grande Valley
Juan Carlos Lopez-Alvarenga
University of Texas Rio Grande Valley
Nitin Das
University of Texas Health Science Center at Tyler: The University of Texas Health Science Center San Antonio
Javad Habibi
University of Missouri Columbia Health Care: MU Health Care
Guanghong Jia
University of Missouri Columbia Health Care: MU Health Care
Guido Lastra
University of Missouri Columbia Health Care: MU Health Care
Bysani Chandrasekar
University of Missouri Columbia Health Care: MU Health Care
Vincent G Demarco (demarcov@missouri.edu)
University of Missouri Columbia https://orcid.org/0000-0003-2092-9995

Original investigation

Keywords: Obesity, Diabetes, Diastolic dysfunction, Neprilysin inhibition

Posted Date: January 5th, 2021

DOI: https://doi.org/10.21203/rs.3.rs-138875/v1

Version of Record: A version of this preprint was published at Cardiovascular Diabetology on April 21st, 2021. See the published version at https://doi.org/10.1186/s12933-021-01270-1.

Sacubitril/valsartan inhibits obesity-associated diastolic dysfunction through suppression of ventricular-vascular stiffness

Annayya R. Aroor[1,2,3], Srinivas Mummidi[4], Juan Carlos Lopez-Alvarenga[4], Nitin Das[5], Javad Habibi[1,2,3], Guanghong Jia[1,2,3], Guido Lastra[1,2,3], Bysani Chandrasekar[3,6,7,8]* and Vincent G. DeMarco[1,2,3,7,8]*

[1]Diabetes and Cardiovascular Center, University of Missouri School of Medicine, Columbia, Missouri, USA
[2] Division of Endocrinology and Metabolism, Department of Medicine, University of Missouri, Columbia, MO, USA
[3]Research Service, Harry S. Truman Memorial Veterans Hospital, Columbia, MO, USA
[4] South Texas Diabetes and Obesity Institute, Department of Human Genetics, School of Medicine, University of Texas Rio Grande Valley, Edinburg, TX, USA
[5]Department of Cardiothoracic Surgery, University of Texas Health Science Center, San Antonio, TX, USA
[6]Division of Cardiovascular Medicine, Department of Medicine, University of Missouri Columbia, MO, USA
[7]Dalton Cardiovascular Research Center, University of Missouri, Columbia, MO, USA
[8]Department of Medical Pharmacology and Physiology, University of Missouri, Columbia, MO, USA

Running Head: LCZ reverses cardiovascular dysfunction in obesity cardiomyopathy

Co-corresponding author	***Corresponding Author:***
Bysani Chandrasekar, DVM, Ph.D.	Vincent G. DeMarco, PhD
Professor of Medicine	Associate Research Professor of Medicine
Department of Medicine	Department of Medicine
Division of Cardiovascular Medicine	Division of Endocrinology and Metabolism
University of Missouri-Columbia School of Medicine	University of Missouri-Columbia School of Medicine
One Hospital Dr	D110, DC043.0
Columbia, MO 65212	One Hospital Dr
chandrasekarb@health.missouri.edu	Columbia, MO 65212

(573) 814-6000 ext 53734	demarcov@missouri.edu (573) 814-6000 ext 53678

Abstract

Objective: Both cardiac diastolic dysfunction (DD) and arterial stiffness are early manifestations of obesity-associated prediabetes and serve as risk factors for the development of heart failure with preserved ejection fraction (HFpEF). Since the incidence of DD and arterial stiffness are increasing worldwide due to exponential growth in obesity, an effective treatment is urgently needed to blunt their development and progression. Here we investigated whether the combination of an inhibitor of neprilysin (sacubitril), a natriuretic peptide-degrading enzyme, and an angiotensin II type 1 receptor blocker (valsartan), suppresses DD and arterial stiffness in an animal model of prediabetes more effectively than valsartan monotherapy.

Methods: Sixteen week-old male Zucker Obese rats (ZO; n=64) were assigned randomly to 4 different groups: Group 1: saline control (ZOC); Group 2: sacubitril/valsartan (sac/val; 68 $mg \bullet kg^{-1} \bullet day^{-1}$; ZOSV); Group 3: valsartan (31 $mg \bullet kg^{-1} \bullet day^{-1}$; ZOV) and Group 4: hydralazine, an anti-hypertensive drug (30 $mg \bullet kg^{-1} \bullet day^{-1}$; ZOH). Six Zucker Lean (ZL) rats that received saline only (Group 5) served as lean controls (ZLC). Drugs were administered daily for 10 weeks by oral gavage.

Results: Sac/val improved echocardiographic parameters of impaired left ventricular (LV) stiffness in untreated ZO rats, without altering the amount of food consumed or body weight gained. In addition to improving DD, sac/val also decreased aortic stiffness and reversed impairment of nitric oxide-induced vascular relaxation seen in ZO rats. However, sac/val had no impact on LV hypertrophy. Notably, sac/val was more effective at ameliorating DD compared to val. Although, hydralazine was as effective as sac/val in improving these parameters, it adversely affected LV mass index. Further, proteomics revealed distinct effects of sac/val, including marked suppression of Notch-1 by both valsartan and sac/val suggesting that cardiovascular protection afforded by both share some common mechanisms;

however, sac/val increased IL-4 which is increasingly been recognized for its cardiovascular protection, possibly contributing, in part, to more favorable effects of sac/val over val alone in improving obesity-associated DD.

Conclusions: These studies suggest that sac/val is superior to val in reversing obesity-associated DD. It is an effective drug combination to blunt progression of asymptomatic DD and vascular stiffness to HFpEF development in a preclinical model of obesity-associated prediabetes.

Key Words: Obesity, Diabetes, Diastolic dysfunction, Neprilysin inhibition

Introduction

Heart failure (HF) with normal or preserved ejection fraction (HFpEF) represents a unique pathophysiological phenotype which is distinct from HF with reduced ejection fraction (HFrEF) [1]. It is associated with structural and functional abnormalities in the heart, characterized by an EF of more than 50% [2]. In this regard, asymptomatic diastolic dysfunction (or preclinical DD) is one of the earliest manifestations during the progression of HFpEF in obesity-associated heart disease in both adults and children [3-5]. Epidemiological studies indicate that nearly two thirds of Americans are overweight or obese and this epidemic is associated with increased cardiovascular disease (CVD)-related morbidity and mortality [6]. The obese population has a high incidence of insulin resistance, that serves as an important risk factor for progression to cardiac dysfunction in the absence of overt coronary heart disease. Moreover, the prevalence of DD is high in the general population and its incidence is further increased in individuals with early phase obesity-associated type 2 diabetes [6, 7] In addition to circulating cytokines or intrinsic structural and functional abnormalities, vascular stiffness also contributes to the development of DD and its progression to HFpEF in obese diabetic individuals [7-11].

There are no evidence-based therapies to treat HFpEF, and therefore therapeutic strategies are urgently needed to improve cardiovascular outcomes, including DD [12]. In this regard, dysregulation of the natriuretic peptide (NP) system and inappropriate activation of the Renin-Angiotensin-Aldosterone System (RAAS) contribute to the development of obesity-associated DD in the absence of significant impairment in EF, a marker of systolic dysfunction [13]. Upregulation of the NP system seen in symptomatic HF is considered as an indication of the response of myocardial tissue to hemodynamic alterations or impaired responsiveness to the effects of NP due to counter regulatory signaling pathways [14-16]. In contrast, NP levels are often lower in the setting of obesity due to either impaired NP

production or its enhanced degradation [17, 18]. Although high doses of NPs are used in the management of acute cardiac dysfunction, their chronic use is limited due to adverse hemodynamic consequences [19]. Inhibition of the RAAS system is considered as one of the therapeutic options for the management of DD, but the long-term administration of angiotensin receptor blockers (ARBs) is associated with aldosterone escape [20, 21]. In this regard, a new class of drug containing the combination of sacubitril, a neprilysin inhibitor that blocks the degradation of NPs, and valsartan, an ARB, is increasingly recognized as an ideal combination to manage HF with reduced EF (HFrEF) [22, 23]. However, little is known regarding the potential of this drug combination (the angiotensin receptor–neprilysin inhibitor; ARNi) to blunt the severity of DD in pre- and early diabetic states of obesity-related cardiomyopathy.

Insulin resistant Zucker Obese (ZO) rats with established DD are extensively used as a genetic model for diet-induced obesity. A leptin receptor mutation in the ZO rat prevents hypothalamic binding of leptin resulting in hyperphagia leading to severe obesity and progression to early stage type 2 diabetes. Similar to cardiovascular manifestations seen in obese humans with cardiorenal metabolic syndrome, ZO rats, at an early age, develop metabolic abnormalities, such as hyperinsulinemia and dyslipidemia that contribute to mild hypertension and an abnormal cardiac phenotype characterized by myocardial interstitial fibrosis, steatosis, abnormal mitochondrial ultrastructure and biogenesis, and DD [24, 25]. Moreover, the development of DD with insulin resistance at an early age in ZO rats also mimics the DD seen in obese young adolescents [5]. We have previously utilized this model to investigate the cellular and molecular mechanisms underlying reversal of obesity-associated DD by several therapeutics, including a DPP-4 inhibitor, mineralocorticoid receptor blocker and an SGLT2 inhibitor [24, 26, 27]. Recently, we reported the beneficial effects of the combination of sacubitril and valsartan (sac/val) in the treatment of early kidney injury in ZO rats [22]. In the present investigation, we investigated whether a ten-week treatment with sac/val (LCZ696) could ameliorate progression of

an already established abnormal cardiac phenotype in ZO rats. Moreover, we evaluated the efficacy of sac/val relative to val monotherapy and the antihypertensive drug, hydralazine. Additionally, we performed proteome analysis to identify potential targets for precision-based therapy. Herein, we report that sac/val, used as a treatment strategy, reduced the severity of DD and improved associated vascular stiffness and endothelial dysfunction in ZO rats relative to val or hydralazine monotherapy by modulating some common as well as distinct molecular targets.

Methods

Animals

Sixty-four male Zucker Obese (ZO) and six age-matched Zucker Lean (ZL) rats were purchased from Charles River Laboratories (Wilmington, MA), and housed in a 12-hour light/dark cycled room. Animals were cared for in accordance with the National Institutes of Health guidelines. All procedures were approved and performed in accordance with the Subcommittee for Animal Safety of the Harry S Truman Veterans Memorial Hospital and the Institutional Animal Care and Use Committee of the University of Missouri. All ZO rats were weighed prior to the start of the experiment and randomly distributed into four treatment groups so that each group had a similar mean body weight. Beginning at 16 weeks of age, ZO rats received sac/val (ZOSV; 68 $mg \bullet kg^{-1} \bullet day^{-1}$), val (ZOV; 31 $mg \bullet kg^{-1} \bullet day^{-1}$), hydralazine (ZOH; 30 $mg \bullet kg^{-1} \bullet day^{-1}$) or saline (ZOC) once daily for 10 weeks by gavage. Rats were gavaged at the same time each morning (6:00-7:00 am central standard time). Body weights were measured every week thereafter until the end of the experiment (26 weeks of age). Untreated age-matched male ZL rats served as lean controls (ZLC). Six rats were removed from the study due to complications associated with oral gavage.

Telemetric blood pressure monitoring

Under isoflurane anesthesia (2% isoflurane in a stream of O_2), a subset of 13 week-old ZO rats (n=16) were implanted with an abdominal aorta catheter attached to a radio transmitter (TA11PA-C40; Data Sciences International, St Paul, Minnesota), as previously described [22, 28]. After a 3-week recovery, both systolic (SBP) and diastolic blood pressures (DBP) were monitored in 300-second bins every 15 minutes for two 12-hour light and two 12-hour dark cycles (sampling rate, 1000 Hz), and telemetry data were analyzed post hoc. Monitoring periods ended 2 days prior to and approximately 3, 5, 7 and 9 weeks after treatment began. One rat was removed from the study prior to the start of BP monitoring due to complications from transmitter implantation surgery. We have previously reported mean arterial pressures in the same rats used in this study [22].

Ultrasound assessment of aortic and cardiac function

Doppler ultrasound (Vevo 2100, Fujifilms, Visualsonics, Toronto, ON, Canada) studies were performed at the Small Animal Ultrasound Imaging Center at the Harry S Truman VA Research Center on isoflurane-anesthetized rats (1.75-2% in 100% oxygen stream) near study end utilizing an MS250 (13-24 MHz) echo probe. Rats were placed on a heated platform to maintain body temperature at 37^{o}C and heart rate of 400 to 450 bpm. In vivo aortic stiffness was evaluated by the transit time method to determine aortic pulse wave velocity (PWV), as previously described [29]. Briefly, PWV was calculated as the difference in arrival times of a Doppler pulse wave at two locations along the aorta at a fixed distance. Pulse wave arrival times are measured as the time from the peak of the ECG R-wave to the leading foot of the pulse wave at which time velocity begins to rise at the start of systole. The measured distance between the two locations along the aorta is divided by the difference in arrival times and is expressed in m/s. Velocity waveforms were acquired at the aortic arch followed

immediately by measurement at the distal descending aorta a known distance from the aortic arch. Next, two-dimensional echocardiograms were performed in the apical four chamber view. In pulse wave (PW) Doppler mode, peak early (E) and late (A) diastolic blood flow velocities were obtained at the level of the mitral inflow stream just proximal to the mitral leaflets. From the PW spectra we determined isovolumic relaxation time (IVRT), isovolumic contraction time (IVCT) and ejection times, parameters needed to calculate the myocardial performance index (MPI), also known as the Tei index. MPI was calculated as the sum of isovolumic contraction and relaxation times divided by ejection time. B- and M-mode images of the left ventricle and septum in short axis view were acquired at the level of the papillary muscles. Left ventricular anterior and posterior wall thicknesses at end systole (LVAWTs and LVPWTs) and diastole (LVAWTd and LVPWTd), luminal diameters (LVIDs and LVIDd) and ejection fraction (EF) were determined offline in M-mode. Next, Tissue Doppler Imaging (TDI) was performed in the apical four chamber view by placing a sample volume at the septal annulus to acquire early (e') and late (a') septal annular velocities. Using a modified parasternal long axis view of the left ventricle and aortic root we determined stroke volume (SV) and cardiac output (CO). A sample volume was placed in the aortic outflow tract to obtain blood velocity spectra in Doppler PW mode. Offline calculation of the velocity time integral of PW traces and measurement of the maximum diameter of the ascending aorta acquired in B-mode were used to calculate SV and CO using onboard software. Parameters were assessed using an average of three heart beats from two to three different spectra, and calculations were made in accordance with the American Society of Echocardiography guidelines as well as specific guidelines for rodent echocardiography. All data were acquired and analyzed offline by a single blinded observer. Although we had previously reported an abnormal diastolic phenotype in young male ZO rats (24, 25 and 29), herein we performed cardiac ultrasound on ten randomly selected ZO rats prior to the beginning of the treatment period (15 weeks old) in order to

determine whether these rats have an abnormal pre-existing cardiac phenotype (**Supplemental Table 1**).

Ex vivo aortic reactivity by wire myography

Vasomotor responses of aortae were examined as previously described [25, 29]. Briefly, a 2 mm segment of thoracic aorta, collected immediately after euthanasia, was placed in ice-cold physiological salt solution (PSS) containing (in mM): 119 NaCl, 4.7 KCl, 2.5 CaCl, 1.18 KH_2PO_4, 1.17 $MgSO_4$, 0.027 EDTA, 5.5 glucose, and 25 $NaHCO_3$, pH 7.4. Aortic contractile state was ascertained using 80 mM KCl. Initially, aortas were preconstricted with U46619 (100 nM), a thromboxane A2 mimetic. Relaxation responses of arterial rings to acetylcholine (1 nM to 100 μM) were assessed by cumulative addition of agonist to the vessel bath. At the end of each experiment, the PSS bath solution was replaced with Ca^{2+}-free PSS to determine maximal passive diameter. Aortic dilator responses are presented as percent maximal relaxation.

Ex vivo endothelial cell (EC) stiffness by atomic force microscopy (AFM)

The stiffness of EC, measured as the force exerted by a stylus probe on the luminal surface of aortic explants, was measured by a nano-indentation technique utilizing AFM, as previously described by us [29]. Briefly, a 2 mm ring of the thoracic aorta was isolated from rats to assess the stiffness of EC. The aortic ring was opened longitudinally, and the adventitial surface of each explant was fastened to a glass cover slip using Cell-tak so that we had en face access to the EC surface for placement of the AFM stylus. Stiffness of the EC surface was estimated by placing the stylus at approximately 15 random locations along the EC surface of an explant and determining the average EC stiffness for that aorta.

Quantification of myocardial interstitial and periarterial fibrosis

Two mm-thick slices of the LV free wall were fixed in paraformaldehyde, embedded in paraffin, sectioned at five microns and stained for collagens using Picro Sirius Red (PSR), as previously described [27]. For each animal, an average estimate of interstitial fibrosis was calculated from four randomly selected regions. Periarterial fibrosis was determined by normalizing the area of PSR stain surrounding an arteriole to arteriolar diameter (diameter = circumference of artery/3.14). Average values for each animal were based on measurements made on four randomly selected coronary arterioles from ZLC (n=6), ZOC (n=5), ZOSV (n=5), ZOV (n=6) and ZOH (n=7).

Analysis of cardiac and aortic 3-nitrotyrosine (3NT)

We evaluated the levels of 3NT as a marker of myocardial nitrosylated oxidation products caused by the formation of peroxynitrite. Five micron sections of the LV free wall were initially quenched of endogenous peroxidase and incubated overnight with rabbit polyclonal anti-3NT antibody (1:200; Chemicon, Temecula, CA). Sections were washed and incubated with appropriate secondary antibody. Diaminobenzidine (DAB; DAKO) served as a chromogen. Using a 50i Nikon microscope, five randomly selected 10X bright-field images from each section were captured with a CoolSNAP cf camera. Signal intensities of brownish color, which is indicative of the 3NT level, were quantified by MetaVue software.

Analysis of intracardiac cytokine protein profile by Quantibody® Rat Cytokine Array 65

Changes in cytokine protein levels in the heart were custom analyzed by RayBiotech using the Rat Cytokine Array Q67 and analyzed using proprietary software. This array is a combination of 2 nonoverlapping arrays that facilitates quantitative measurement of the concentrations of 67 rat

cytokines by using appropriate antibody pairs. Within the array, an individual cytokine was represented four times, along with positive and negative controls which allows for calculating standard deviation. Differences in cytokine expression were expressed as $\log_2$ fold changes. Unpaired two-tailed t-tests were used to determine the significance ($p < 0.05$) of differentially expressed cytokines between different groups (e.g., ZOC versus ZOSV, ZOV or ZOH). Cytokines that exhibited statistically significant differences between the treatment and control groups were selected for input into Ingenuity Pathway Analysis (IPA, Qiagen, Germantown, MD) to identify diseases and functions that were affected. Heatmaps were generated using the ggplot2 package for R.

Statistical Analysis

Results are reported as the mean ± SE. One-way ANOVA and post hoc t-tests (Fisher's LSD), or corresponding non-parametric Kruskal-Wallis (Dunn's), as indicated, were performed to examine differences in outcomes between ZL rats and control and treated ZO groups. Alternatively, we performed two-tailed Student t-tests between two groups when ANOVA post hoc tests indicated p=0.10. A p value <0.05 was considered significant. Two-way ANOVA was used to compare aortic responses among groups to increasing concentrations of acetylcholine in the tissue bath (group x Ach concentration). Differences in systolic or diastolic blood pressure at the last measurement period following administration of sac/val, val or hydralazine versus untreated ZO rats were determined by Student t-tests adjusted by variance. Sample sizes are listed in tables and figures. The heatmaps were normalized by scaling the values using the sum of each row. The z-scores were calculated with the Creative Commons Attribution-ShareAlike 2.0 Generic from the University of Alberta, Canada.

Results

Blood pressure and baseline metabolic parameters

We previously reported baseline metabolic parameters and 24-h ambulatory mean arterial pressures in the same cohort of rats utilized in the present study [22]. The changes in systolic and diastolic blood pressure and their relation to light and dark cycle are presented in **Fig. 1**. Briefly, compared to ZLC, ZOC exhibited increases in body weight, fat pad mass, fasting glucose, fasting insulin and insulin resistance (assessed by Homeostatic Model Assessment of Insulin Resistance or HOMA-IR) ($p<0.05$), and these parameters were largely unaffected by sac/val, val or hydralazine. However, in that study, we also reported that the ZOV group had the highest HbA1c, fasting glucose and insulin resistance of the five groups of rats examined [22].

Structural remodeling and diastolic dysfunction

We previously reported cardiac hypertrophy and DD in male ZO rats as young as nine weeks of age [24, 25, 30]. Herein, we determined that 10 randomly selected ZOC exhibited cardiac hypertrophy and an abnormal diastolic phenotype before treatment was initiated (**Table 1**), indicating that the study is directed as a treatment strategy rather than a prevention strategy.

At the end of the study period, untreated ZO rats (ZOC) exhibited cardiac hypertrophy indicated by increases in heart weight (HW) (25%), HW normalized to tibia length (HW/TL) (72%), left ventricular (LV) mass (24%), and anterior wall thickness at end diastole (AWTd) (29 %) compared age-matched non-diabetic, Zucker Lean rats (ZLC) (**Table 2**). ZOC and ZLC exhibited ejection fractions ≥ 69% indicating normal systolic function. However, compared to ZLC, ZOC exhibited DD characterized by a decrease in the tissue Doppler derived e'/a' ratio (38%), in concert with increases in LV filling pressure (E/e' ratio, 220%), diastolic stiffness (E/e'/LVIDd, 230%), isovolumic relaxation

time (IVRT, 47%) and the myocardial performance index (MPI, 23%). Collectively, these parameters demonstrate abnormal LV wall motion during diastole (e'/a' and E/e'), passive LV wall stiffness (E/e'/LVIDd) and prolongation of the active energy requiring period of relaxation (IVRT). Additionally, DD in ZOC was associated with left atrial remodeling indicated by an increase in the left atrial to aortic root (LA/Ao) ratio (45%), an effect that reflects the response by the thin walled atrium to increased luminal pressure.

Although untreated ZO rats (ZOC) exhibited cardiac hypertrophy indicated by increases in HW, LV mass, and AWTd, these parameters were not altered by sac/val (ZOSV), val alone (ZOV), or hydralazine (ZOH) (**Table 2**). However, a moderate, but significant, degree of fibrosis in the interstitial region was seen in ZOC compared to ZLC (**Fig. 2A**). Though sac/val, val and hydralazine were all effective in decreasing fibrosis in ZO rats, the magnitude of decease was not different between the three treated groups. The extent of fibrosis in periarterial region was increased in ZOC rats (**Fig. 2B**) and was decreased significantly in ZOSV and ZOV. The area of fibrosis was not significantly decreased in ZOH.

The comparison of different parameters of DD in ZOC and the treated groups is summarized in **Table 2**. Compared to ZOC, the e'/a' ratio improved by 42% in ZOSV and 47% in ZOH, but not in ZOV (-1%). Indeed, ZOV was significantly lower than in ZOC, ZOL and ZOH. Compared to ZOC, LV filling pressure (E/e') was lower by 25, 8 and 32% in ZOSV, ZOV and ZOH, respectively, although the differences were not significant. Similarly, compared to ZOC, diastolic stiffness index (E/e'/LVID) was lower by 22, 6 and 38% in ZOSV, ZOV and ZOH, respectively. IVRT was significantly reduced (improved) by 17, 21 and 29% in ZOSV, ZOV and ZOH, respectively, compared to ZOC. MPI, which is an index of global cardiac function (*i.e.*, diastolic and systolic), was improved by 16, 10 and 10% in ZOSV, ZOV and ZOH, respectively, however only ZOSV was significantly lower than ZOC. Sac/val

tended to improve diastolic stiffness index and improved e'/a' ($p<0.05$) ratio compared to val. Although hydralazine is as effective as sac/val at improving DD parameters, it causes significant increase in LVMI which is considered to contribute to progression of cardiac dysfunction.

Oxidative stress

Oxidative stress is one of the important determinants that either precedes or is associated with the development of DD in rodent models of obesity-associated cardiomyopathy [28, 31]. We have evaluated oxidative stress by analyzing the extent of 3-nitrotyrosine (3NT) accumulation in both interstitial and periarterial regions in the heart. Accumulation of 3NT in interstitium is increased in untreated ZO rats ($p, <0.05$ vs ZLC), but decreased in all three treatment groups (**Fig. 3A**) ($p<0.05$ versus ZOC). In contrast to interstitial 3NT accumulation, periarterial 3NT was marginally increased in ZO rats compared to control ZLC rats ($p=0.06$), and neither sac/val, val or hydralazine had a significant effect on periarterial nitroso-oxidative stress (**Fig. 3B**).

Aortic stiffness and relaxation

We have determined aortic compliance by measuring in vivo pulse wave velocity (PWV) and ex vivo aortic stiffness by atomic force microscopy (AFM) in aortic explants. Compared to untreated ZO rats, PWV was decreased similarly in all three treatment groups ($p<0.05$) (**Fig. 4A**). Endothelial cell surface stiffness was also significantly decreased in ZOSV, ZOV and ZOH groups compared ZOC group (**Fig. 4B**). We further examined endothelial dependent aortic relaxation. We previously reported impaired endothelium-dependent vasodilation in younger and older ZO rats [24, 28]. We anticipated impaired endothelium-dependent vasodilatory responses to acetylcholine and insulin in the aorta of ZOC and improvement with sac/val, to a greater extent than to val or hydralazine. As expected, acetylcholine-induced vasodilation was significantly lower in ZOC relative to ZLC (**Fig. 4C**). However, treatment

with sac/val or val, but not hydralazine, showed normal responses to acetylcholine, and are similar to ZLC. Responses to insulin and the endothelium-independent vasodilator, sodium nitroprusside were not different among the groups tested (not shown).

Cytokine measurements

To explore the molecular mechanisms in the ZLC, ZOC, ZOSV, and ZOV groups (N=4 in each group) that could potentially mediate the functional/structural changes in the heart, we used a commercial service to measure 67 cytokines using a Cytokine Array. Given the exploratory nature of these experiments and the small sample size, we did not adjust the significance values for multiple testing and p-value ≤ 0.05 was considered significant. We found that five cytokines, namely RANTES, PDGF-AA, GFR alpha-1, SCF, and IL-7, were differentially expressed between the lean (ZLC) and obese (ZOC) rats (**Table 3**). Relative to the ZOC rats, the ZOV rats showed downregulation of five proteins, namely, Neuropilin-1, Notch-1, JAM-A, RANTES, and Flt-3L (**Table 4**). Remarkably, the ZOSV rats showed reduced expression of Neuropilin-1, Notch-1, and JAM-A relative to ZOC rats which was similar to that seen in ZOV rats (**Table 4**). In addition, the ZOSV rats showed increased expression of PDGF-AA, L-Selectin, IFN-γ, and IL-4 when compared to the ZOC rats. A heatmap of the relative differences of statistically significant cytokines in cardiac lysates across the ZOC, ZOV, and ZOSV rats is shown in **Fig. 5**. The increased expression of the aforementioned four proteins distinguishes ZOSV rats from ZOV rats suggesting that they could potentially mediate the effects associated with sac/val treatment.

IPA analysis

We then sought to map the differentially expressed cytokines detected in the ZOL rats to the networks that may mediate the effects of sac/val that are accessible through the Ingenuity database. We did not perform a similar analysis for the ZOV rats as only five cytokines were differentially expressed in these rats relative to ZOC and three of them were also present in the ZOL rats. Our analysis generated a single network with a score of 21 with the following associated functions: cellular development, cellular movement, cellular growth, and proliferation **(Fig. 6**). The network included the following focus (experimentally detected) molecules: NOTCH-1, IL-4, IFN-γ, PDGFA, F11R, L-Selectin (SELL), and NRP1. Remarkably, one of the focus molecules of the network is Notch-1, a key player in vascular remodeling and endothelial and SMC communication. The cellular and molecular functions of the molecules in the network were related to cell morphology, cell movement, cell death and survival. cell-to-cell signaling and interaction, and cellular development. The top disease and functional annotation of these molecules is the inflammatory response (P = 2.54E-04 - 1.79E-10) and are related to macrophage polarization (P = 1.79 E-10) and leukocyte emigration (P = 1.07E-9). Of note, mapping these molecules to clinical pathology endpoints suggested an association with cardiac enlargement (P = 6.41E-02 - 6.20E-05). The top canonical pathways predicted were the Th1 (P = 5.07E-06) and Th2 pathways (P = 7.20E-06). Notably, IL-4 that anchors Th2 pathway plays a key role in macrophage polarization that is important in vascular remodeling.

DISCUSSION

In the present investigation, we examined the potential therapeutic effects of sacubitril/valsartan (sac/val; LCZ696), a combination of Ang II receptor blocker and neprilysin (NEP) inhibitor (ARNi), on cardiovascular remodeling and function in pre-diabetic obese rats. We then compared the effects of dual blockade (sac/val) with val monotherapy, and to those of hydralazine, a blood pressure lowering

drug, to determine the cardiovascular protection. Furthermore, we performed proteome array analysis of selected proteins showing differences in distinct signaling pathways. For the first time, we have shown the enhanced cardiovascular protection afforded by sac/val on selective parameters of diastolic function, as well systolic function, and large artery stiffness compared to val and hydralazine.

Diastolic dysfunction (DD), characterized by impaired relaxation of the left ventricle, is one of the early manifestations of heart failure with preserved ejection fraction (HFpEF) [32, 33]. Childhood-adolescent overweight and obesity are major health burdens around the globe and the presence of DD has significant impact as a risk factor for the progression of CVD [6, 7]. However, drugs targeting systolic dysfunction are not usually considered as effective in the management of DD, thereby necessitating the need to develop drugs that specifically target DD, especially in the setting of obesity [34, 35]. In this regard, obesity-induced DD is associated with multiple abnormalities, including inappropriate activation of tissue renin-angiotensin-aldosterone system (RAAS) [24, 36, 37], as well as, normal or subnormal responses to ANP in the early stages of the disease or enhanced ANP responsiveness at later stages [23]. Sac/val is a first-in-class approved ARNi, that simultaneously provides Ang II type I receptor blockade and NP inhibition. Although, the cardiac protection afforded by sac/val is well recognized with completion of first and second phase clinical trials [1], the benefits of sac/val in HFpEF needs further evaluation. In fact, recent analysis of sac/val in heart failure with reduced ejection fraction (HFrEF) suggests that, improvements are more significant with the drug if the systolic dysfunction is not severe, suggesting the need for early detection and management of HFrEF [38-41]. Recent study has also favored the beneficial effects of sac/val in HFpEF patients [42]. Therefore, we have chosen Zucker Obese rats, a preclinical model of early DD, to represent young patients with cardiometabolic syndrome with a constellation of features, including hypertension,

hyperlipidemia and insulin resistance [43]. We then compared the efficacy of sac/val with val alone and with hydralazine, a blood pressure lowering agent.

All three drugs, sac/val, val and hydralazine, improved IVRT, a parameter of prolongation of the active energy phase of relaxation. However, impairment in LV wall motion during diastole, observed in untreated ZOC rats and indicated by an increase in the e'/a' ratio, was improved by sac/val, but not val. Moreover, sac/val, but not val, tended to improve passive LV wall stiffness (E/e'/LVIDd). MPI (Myocardial Performance Index), which is an index of global cardiac function (*i.e.*, diastolic and systolic), was significantly improved only by sac/val, potentially due in part to improvement in IVCT. Taken together, sac/val treatment appears to be superior in improving DD in this preclinical model of obesity cardiomyopathy. Interestingly, the enhanced efficacy of sac/val occurred without significant improvement in blood glucose or insulin levels and suggests that these benefits occur independent of glycemic control.

The factors contributing to HFpEF in contrast to HFrEF have been related to multiple factors, including endothelial dysfunction, changes in intrinsic cardiomyocyte stiffness with relaxation abnormalities, and low-grade metabolic inflammation with variable extent of fibrosis and oxidative stress [44-47]. We have evaluated myocardial oxidative stress, as determined by 3NT accumulation, as an index of superoxide production and the generation of reactive nitrogen species, by immunohistochemistry. Cardiac fibrosis, intrinsic stiffness and hypertrophy have all been shown to be caused, in part, by enhanced ROS generation in the cardiovascular tissue [11, 48, 49]. Although we found suppression of ROS in LV interstitium by all three drugs, it was not significantly different between the drug-treated groups. This finding suggests that suppression of oxidative stress may, in part, contribute to improvement in DD, and the beneficial effects of sac/val may be mediated by factors

independent of ROS accumulation. We therefore performed cytokine proteome array which is an emerging technology being used to analyze DD in metabolic disease [50-52].

The analysis revealed, among other things, that Notch-1 is markedly decreased by both sac/val and val. However, it appears that the effects of Notch-1 are cell type-specific. For example, Notch-1 exerts protective effects in endothelial cells and cardiomyocytes, but plays a deleterious role in fibroblasts and immune cells [53, 54]. Interestingly, both ZOSV and ZOV showed improvement in DD and suppressed Notch-1 expression, suggesting that the beneficial effects of sac/val and val in the ZO model of obesity-associated DD may be, in part, explained by suppression of Notch-1 in fibroblasts and immune cells. However, ZOSV showed increased expression of IFN-γ compared to the other groups. Although IFN-γ is implicated in immune and inflammatory responses as a component of the Th1 response, its increased expression has been shown to exert contrasting effects; promote cardiovascular dysfunction or mediate cardioprotective effects [55-60]. However, unlike in other studies [56-60], changes in IFN-γ levels did not correlate with suppression of cardiac hypertrophy in the sac/val-treated ZO rats. IL-4 levels were also elevated in ZOSV, but not in other treatment groups, suggesting that increased IL-4 levels in this treated group might have contributed to the higher impact of sac/val over val in ZO rats. In fact, IL-4 is emerging as a cardioprotective and repurposing molecule to improve cardiac dysfunction by promoting M2 macrophage polarization and suppression of cardiac inflammatory response [61, 62]. Therefore, it is plausible that upregulation in IL-4 signaling in the sac/val treated ZO rats might have contributed to further improvements in DD compared to val alone. The cytokine array also revealed that RANTES expression is suppressed in untreated and all treated groups, and more so in the ZOV group. In this regard, hyperinsulinemia as seen in ZO rats might have contributed to suppression of RANTES, although its role in DD is not fully understood [63, 64]. However, a limitation of our cross-sectional study design is that it does not capture the dynamic

changes in the cytokine profile over the treatment period. In the future, we will include a longitudinal study design to gain further mechanistic insights into the beneficial effects of sac/val treatment.

It is well established that persistent AT_1 receptor activation promotes endothelial dysfunction and cardiovascular fibrotic response where natriuretic peptides are known to counter these deleterious effects [65]. Two critical determinants of these effects are bioavailable nitric oxide and cyclic GMP generation [66]. While Ang II could decrease bioavailable nitric oxide by causing insulin-mediated impairment of eNOS activation and nitric oxide destruction, an increase in cyclic GMP by ANP will further enhance accumulation of cyclic GMP with a concomitant increase in nitric oxide production and signaling [26]. In addition, intrinsic cardiomyocyte stiffness is also regulated by cyclic GMP dependent phosphorylation of titin protein in cardiomyocytes [67, 68]. Therefore, additional provision of cyclic GMP by sac/val compared to val alone might have contributed to further improvements in diastolic function observed in this study.

Additional risk factors like hypertension and myocardial hypertrophy also contribute to DD. Surprisingly, all three drugs decreased blood pressure to a similar extent, suggesting that the cardioprotective effects afforded by sac/val appear to be independent of changes in blood pressure. Although increased blood pressure has shown a strong association with obesity cardiomyopathy, RAAS activation-induced DD may occur through enhanced oxidative stress and profibrotic effects rather than through regulation of blood pressure [69]. Moreover, we did not find improvements in structural abnormalities, including cardiac hypertrophy, by sac/val or val, suggesting further that improvement in diastolic function occurs independent of improvements in structural remodeling. In fact, improvement in diastolic function, independent of changes in hypertrophy and structural remodeling, has been reported in both preclinical models of obesity cardiomyopathy and human patients [28, 70].

Sac/val (ARNi) therapy has recently been shown to improve aortic compliance in heart failure patients [71]. Our results also show that sac/val significantly improved aortic compliance by decreasing aortic stiffness, as evaluated by PWV. Aortic stiffness is associated with components of the cardiorenal metabolic syndrome [9, 11, 72, 73]. Although arterial stiffness increases with aging, the process is accelerated and occurs earlier in the presence of obesity, insulin resistance and diabetes. Therefore, arterial stiffness is emerging as an important risk factor and a target for improved outcomes in cardiovascular disease and chronic kidney disease, specifically in those with obesity and diabetes. Increased systolic pressure and decreased diastolic pressure result in increased pulse pressure caused by stiffening of central arteries. An increase in systolic pressure causes an increase in cardiac afterload, left ventricular mass, and oxygen demand, whereas decreased diastolic pressure impairs coronary blood flow. These changes can result in left ventricular remodeling, ischemia and fibrosis, all of which contribute to left ventricular diastolic dysfunction and coronary heart disease [9].

Improvement in aortic stiffness is often associated with better vascular health, and in turn diastolic function. Here, we used acetylcholine-dependent aortic relaxation as a surrogate for nitric oxide-dependent endothelial function. We observed improved acetylcholine-dependent vasorelaxation by sac/val and val. However, no such improvement was seen with hydralazine. PWV and endothelial surface stiffness measure overall stiffness of the vascular wall of aorta which was decreased by hydralazine, suggesting dissociation between vascular stiffness and nitric oxide-dependent vasodilatation. In this regard, we have previously reported impaired microvascular remodeling as shown by increased RRI and renovascular fibrosis by hydralazine, but not sac/val and val [22]. In this study, we also observed perivascular fibrosis in the hydralazine treated ZO rats along with enhanced left ventricular mass suggesting increased strain on the part of ventricles, in part, due to microvascular stiffening by hydralazine. In this regard, it is noteworthy that although hydralazine is used in the

management of hypertension, it is also known to suppress acetylcholine-induced vasorelaxation as observed in the present study [74].

Conclusion

The prognosis of patients diagnosed with heart failure with preserved ejection fraction (HFpEF) remains poor, specifically in patients with comorbid conditions like obesity. Further, there are no evidence-based therapies to treat HFpEF. Therefore, therapeutic strategies are urgently needed to improve cardiovascular outcomes in subjects with HFpEF, including diastolic dysfunction [12]. Using a preclinical model of obesity and pre-diabetes, here we report that sacubitril/valsartan (sac/val; LCZ696), a combination of Ang II receptor blocker and neprilysin (NEP) inhibitor (ARNi), improved echocardiographic parameters of ventricular stiffness that were impaired in untreated ZO rats. Moreover, sac/val was more effective at ameliorating diastolic dysfunction compared to val alone. Sac/val also blunted elevated vascular stiffness in ZO rats more effectively than val monotherapy. Although the antihypertensive drug hydralazine was as effective as sac/val in improving parameters of diastolic function, it failed to affect periarterial fibrosis and aortic compliance. While the immune suppressive effects of sac/val treatment are well recognized, our proteomic analysis also suggests that this drug combination can have protective effects on DD through a previously unrecognized effect on IL-4 induction. Thus sac/val treatment may contribute to improvement in cardiovascular stiffness through both common and novel pathways involving immune suppression and tissue repair. Our results also show that the sac/val combination improved diastolic function better than val monotherapy, suggesting a role for enhanced cardiac cyclic GMP signaling. Taken together, these studies suggest that sac/val is superior to val in reversing obesity-associated DD, and is an attractive drug combination for

the treatment of early asymptomatic diastolic dysfunction in obesity and prevention of progression of CVD leading to HFpEF.

Abbreviations

ACEi: ACE inhibitor; AFM, atomic force microscopy; ARB: angiotensin type 1 receptor (AT1R) blocker; ANP: atrial natriuretic peptide; ARNI, angiotensin receptor-neprilysin inhibition; cGMP: cyclic guanosine monophosphate; CV: cardiovascular; CVD: CV disease; DAB: diaminobenzidine; DBP, diasotolic blood pressure; DD, diastolic dysfunction; DPP4: dipeptidyl peptidase 4; ECG, electrocardiogram; EF, ejection fraction; HFpEF: heart failure with preserved ejection fraction; HFrEF: heart failure with reduced ejection fraction; HOMA-IR: homeostatic model assessment of insulin resistance; IL, interleukin; IVRT, isovolumic relaxation time; eNOS, endothelial nitric oxide synthase; 3-NT: 3-nitrotyrosine; LV, left ventricle; NEPi: neprilysin inhibition; Notch-1, Notch I receptor; PSR: picrosirius red; NP, natriuretic peptide; PWV, pulse wave velocity; RRI: renal resistivity index; sac: sacubitril; val: valsartan; sacubitril/valsartan: sac/val; SBP, Systolic blood pressure; RAAS: renin-angiotensin-aldosterone system; SGLT2, sodium/glucose cotransporter 2; T2DM: type 2 diabetes mellitus; ZLC: Zucker Lean control; ZOC: Zucker Obese control; ZOSV: Zucker Obese sac/val; ZOV: Zucker Obese valsartan; ZOH: Zucker Obese hydralazine.

Authors' contributions

VGD conceived study design and experiments; ARA, GJ, NAD, JH, GL, BC, and VGD collected data; SM and JC L-A performed the IPA analysis; VGD, ARA, GJ, BC, SM, JCL-A carried

out data interpretation. All authors were involved in writing the paper and had final approval of the submitted and published versions. All authors read and approved the final manuscript.

Author details

[1]Diabetes and Cardiovascular Center, University of Missouri School of Medicine, Columbia, Missouri, USA; [2] Division of Endocrinology and Metabolism, Department of Medicine, University of Missouri, Columbia, MO, USA; [3]Research Service, Harry S. Truman Memorial Veterans Hospital, Columbia, MO, USA; [4] South Texas Diabetes and Obesity Institute, Department of Human Genetics, School of Medicine, University of Texas Rio Grande Valley, Edinburg, TX, USA; [5]Department of Cardiothoracic Surgery, University of Texas Health Science Center, San Antonio, TX, USA; [6]Division of Cardiovascular Medicine, Department of Medicine, University of Missouri Columbia, MO, USA; [7]Dalton Cardiovascular Research Center, University of Missouri, Columbia, MO, USA; [8]Department of Medical Pharmacology and Physiology, University of Missouri, Columbia, MO, USA

Acknowledgements

Technical assistance was provided by Dongqing Chen, Brady Barron, Mona Katcher, Matt Martin, Sherrie Neff and Justin Wilson. We also appreciate the assistance provided by the Small Animal Ultrasound Imaging Center (SAUIC), located at the Harry S Truman Veterans Memorial Hospital, Columbia, MO, as well as the VA Research and Development Office and the Missouri Foundation for Veteran's Medical Research. We also thank the Clinical Pathology Laboratory at the University of Missouri, School of Veterinary Medicine, for performing plasma and urine assays.

Competing interests

VGD reports having received investigator initiated funding from Novartis, otherwise the authors have nothing to report.

Availability of data and materials

The datasets used and/or analyzed during the current study are available from the corresponding author on reasonable request.

Consent of publication

Not applicable.

Ethics approval and consent to participate

This study was approved by the Subcommittee for Animal Safety of the Harry S Truman Veterans Memorial Hospital and the Institutional Animal Care and Use Committee of the University of Missouri-Columbia.

Funding

This research was supported by an investigator-initiated Grant from Novartis and by the Harry S. Truman VA Medical Research Foundation, Columbia, MO to VGD (LCZ696BUSNC12T). BC is a Research Career Scientist (IK6BX004016) and his work is supported by the VA ORD-BLRD Service Award I01-BX004220. Work in SM's laboratory is supported by NIH/NIAID R01AI119131. Work in GL's laboratory is supported by the Department of Veterans Affairs Merit System (2I01BX001981-

05A1). Work in GJ's laboratory is supported by the National Institute of Diabetes and Digestive and Kidney Diseases (DK124329).

References

1. Lin, X. and L. Fang, *Pharmaceutical Treatment for Heart Failure.* Adv Exp Med Biol, 2020. **1177**: p. 269-295.
2. Branca, L., et al., *Heart failure with mid-range ejection fraction: pro and cons of the new classification of Heart Failure by European Society of Cardiology guidelines.* ESC Heart Fail, 2020. **7**(2): p. 381-399.
3. Santos, J.L., et al., *Subclinical regional left ventricular dysfunction in obese patients with and without hypertension or hypertrophy.* Obesity (Silver Spring), 2011. **19**(6): p. 1296-303.
4. Yoon, Y.S., et al., *Progressive attenuation of myocardial vascular endothelial growth factor expression is a seminal event in diabetic cardiomyopathy: restoration of microvascular homeostasis and recovery of cardiac function in diabetic cardiomyopathy after replenishment of local vascular endothelial growth factor.* Circulation, 2005. **111**(16): p. 2073-85.
5. Van Putte-Katier, N., et al., *Early cardiac abnormalities in obese children: importance of obesity per se versus associated cardiovascular risk factors.* Pediatr Res, 2008. **64**(2): p. 205-9.
6. Sowers, J.R., A. Whaley-Connell, and M.R. Hayden, *The Role of Overweight and Obesity in the Cardiorenal Syndrome.* Cardiorenal Med, 2011. **1**(1): p. 5-12.
7. Nikolajevic Starcevic, J., M. Janic, and M. Sabovic, *Molecular Mechanisms Responsible for Diastolic Dysfunction in Diabetes Mellitus Patients.* Int J Mol Sci, 2019. **20**(5).

8. Zhang, Y., et al., *Effects of exercise modalities on central hemodynamics, arterial stiffness and cardiac function in cardiovascular disease: Systematic review and meta-analysis of randomized controlled trials.* PLoS One, 2018. **13**(7): p. e0200829.

9. Aroor, A.R., G. Jia, and J.R. Sowers, *Cellular mechanisms underlying obesity-induced arterial stiffness.* Am J Physiol Regul Integr Comp Physiol, 2018. **314**(3): p. R387-R398.

10. Weismann, C.G., et al., *Aortic stiffness and left ventricular diastolic function in children with well-functioning bicuspid aortic valves.* Eur Heart J Cardiovasc Imaging, 2016. **17**(2): p. 225-30.

11. Aroor, A.R., et al., *The role of tissue Renin-Angiotensin-aldosterone system in the development of endothelial dysfunction and arterial stiffness.* Front Endocrinol (Lausanne), 2013. **4**: p. 161.

12. Reddy, Y.N.V., et al., *A Simple, Evidence-Based Approach to Help Guide Diagnosis of Heart Failure With Preserved Ejection Fraction.* Circulation, 2018. **138**(9): p. 861-870.

13. Diez, J., *Chronic heart failure as a state of reduced effectiveness of the natriuretic peptide system: implications for therapy.* Eur J Heart Fail, 2017. **19**(2): p. 167-176.

14. Volpe, M., A. Battistoni, and S. Rubattu, *Natriuretic peptides in heart failure: Current achievements and future perspectives.* Int J Cardiol, 2019. **281**: p. 186-189.

15. Grieco, P. and I. Gomez-Monterrey, *Natural and synthetic peptides in the cardiovascular diseases: An update on diagnostic and therapeutic potentials.* Arch Biochem Biophys, 2019. **662**: p. 15-32.

16. Fu, S., et al., *Synthesis, secretion, function, metabolism and application of natriuretic peptides in heart failure.* J Biol Eng, 2018. **12**: p. 2.

17. Bartels, E.D., et al., *Decreased expression of natriuretic peptides associated with lipid accumulation in cardiac ventricle of obese mice.* Endocrinology, 2010. **151**(11): p. 5218-25.

18. Obokata, M., et al., *Evidence Supporting the Existence of a Distinct Obese Phenotype of Heart Failure With Preserved Ejection Fraction.* Circulation, 2017. **136**(1): p. 6-19.

19. Agrawal, V., et al., *Natriuretic peptide receptor C contributes to disproportionate right ventricular hypertrophy in a rodent model of obesity-induced heart failure with preserved ejection fraction with pulmonary hypertension.* Pulm Circ, 2019. **9**(4): p. 2045894019878599.

20. Te Riet, L., et al., *Hypertension: renin-angiotensin-aldosterone system alterations.* Circ Res, 2015. **116**(6): p. 960-75.

21. Lantis, A.C., et al., *Aldosterone breakthrough with benazepril in furosemide-activated renin-angiotensin-aldosterone system in normal dogs.* J Vet Pharmacol Ther, 2015. **38**(1): p. 65-73.

22. Habibi, J., et al., *The combination of a neprilysin inhibitor (sacubitril) and angiotensin-II receptor blocker (valsartan) attenuates glomerular and tubular injury in the Zucker Obese rat.* Cardiovasc Diabetol, 2019. **18**(1): p. 40.

23. Kuchulakanti, P.K., *ARNI in cardiovascular disease - current evidence and future perspectives.* Future Cardiol, 2020.

24. Bender, S.B., et al., *Mineralocorticoid Receptor Antagonism Treats Obesity-Associated Cardiac Diastolic Dysfunction.* Hypertension, 2015. **65**: p. 1082-1088.

25. Manrique, C., et al., *Dipeptidyl peptidase-4 inhibition with linagliptin prevents western diet-induced vascular abnormalities in female mice.* Cardiovasc Diabetol, 2016. **15**: p. 94.

26. Aroor, A.R., et al., *Dipeptidyl peptidase-4 (DPP-4) inhibition with linagliptin reduces western diet-induced myocardial TRAF3IP2 expression, inflammation and fibrosis in female mice.* Cardiovasc Diabetol, 2017. **16**(1): p. 61.

27. Habibi, J., et al., *Sodium glucose transporter 2 (SGLT2) inhibition with empagliflozin improves cardiac diastolic function in a female rodent model of diabetes.* Cardiovasc Diabetol, 2017. **16**(1): p. 9.

28. Aroor, A.R., et al., *Dipeptidylpeptidase Inhibition is Associated with Improvement in Blood Pressure and Diastolic Function in Insulin Resistant Male Zucker Obese Rats.* Endocrinology, 2013. **154**(7): p. 2501-13.

29. Aroor, A.R., et al., *Glycemic control by the SGLT2 inhibitor empagliflozin decreases aortic stiffness, renal resistivity index and kidney injury.* Cardiovasc Diabetol, 2018. **17**(1): p. 108.

30. Zhou, X., et al., *Nebivolol improves diastolic dysfunction and myocardial remodeling through reductions in oxidative stress in the Zucker obese rat.* Hypertension, 2010. **55**(4): p. 880-8.

31. Demarco, V.G., et al., *Obesity-related alterations in cardiac lipid profile and nondipping blood pressure pattern during transition to diastolic dysfunction in male db/db mice.* Endocrinology, 2013. **154**(1): p. 159-71.

32. Kanagala, P., et al., *Characterizing heart failure with preserved and reduced ejection fraction: An imaging and plasma biomarker approach.* PLoS One, 2020. **15**(4): p. e0232280.

33. Bayes-Genis, A., et al., *Transitioning from Preclinical to Clinical Heart Failure with Preserved Ejection Fraction: A Mechanistic Approach.* J Clin Med, 2020. **9**(4).

34. Wintrich, J., et al., *Therapeutic approaches in heart failure with preserved ejection fraction: past, present, and future.* Clin Res Cardiol, 2020.

35. Srivastava, G., et al., *Clinical Considerations Regarding the Use of Obesity Pharmacotherapy in Adolescents with Obesity.* Obesity (Silver Spring), 2019. **27**(2): p. 190-204.

36. Kuno, T., et al., *Meta-Analysis Evaluating the Effects of Renin-Angiotensin-Aldosterone System Blockade on Outcomes of Heart Failure With Preserved Ejection Fraction.* Am J Cardiol, 2020. **125**(8): p. 1187-1193.

37. Pugliese, N.R., S. Masi, and S. Taddei, *The renin-angiotensin-aldosterone system: a crossroad from arterial hypertension to heart failure.* Heart Fail Rev, 2020. **25**(1): p. 31-42.

38. Ksiazczyk, M. and M. Lelonek, *Angiotensin receptor/neprilysin inhibitor-a breakthrough in chronic heart failure therapy: summary of subanalysis on PARADIGM-HF trial findings.* Heart Fail Rev, 2020. **25**(3): p. 393-402.

39. Polito, M.V., et al., *Clinical and echocardiographic benefit of Sacubitril/Valsartan in a real-world population with HF with reduced ejection fraction.* Sci Rep, 2020. **10**(1): p. 6665.

40. Correale, M., et al., *Sacubitril/valsartan improves right ventricular function in a real-life population of patients with chronic heart failure: The Daunia Heart Failure Registry.* Int J Cardiol Heart Vasc, 2020. **27**: p. 100486.

41. Sokos, G.G. and A. Raina, *Understanding the early mortality benefit observed in the PARADIGM-HF trial: considerations for the management of heart failure with sacubitril/valsartan.* Vasc Health Risk Manag, 2020. **16**: p. 41-51.

42. Cunningham, J.W., et al., *Effects of Sacubitril/Valsartan on N-Terminal Pro-B-Type Natriuretic Peptide in Heart Failure With Preserved Ejection Fraction.* JACC Heart Fail, 2020. **8**(5): p. 372-381.

43. Takatsu, M., et al., *Calorie restriction attenuates cardiac remodeling and diastolic dysfunction in a rat model of metabolic syndrome.* Hypertension, 2013. **62**(5): p. 957-65.

44. Simmonds, S.J., et al., *Cellular and Molecular Differences between HFpEF and HFrEF: A Step Ahead in an Improved Pathological Understanding.* Cells, 2020. **9**(1).

45. Camici, P.G., et al., *Coronary microvascular dysfunction in hypertrophy and heart failure.* Cardiovasc Res, 2020. **116**(4): p. 806-816.

46. Franssen, C., et al., *Myocardial Microvascular Inflammatory Endothelial Activation in Heart Failure With Preserved Ejection Fraction.* JACC Heart Fail, 2016. **4**(4): p. 312-24.

47. Loredo-Mendoza, M.L., et al., *The role of inflammation in driving left ventricular remodeling in a pre-HFpEF model.* Exp Biol Med (Maywood), 2020. **245**(8): p. 748-757.

48. Jia, G., V.G. DeMarco, and J.R. Sowers, *Insulin resistance and hyperinsulinaemia in diabetic cardiomyopathy.* Nat Rev Endocrinol, 2016. **12**(3): p. 144-53.

49. Sletten, A.C., L.R. Peterson, and J.E. Schaffer, *Manifestations and mechanisms of myocardial lipotoxicity in obesity.* J Intern Med, 2018. **284**(5): p. 478-491.

50. Altara, R., et al., *In Silico Analysis of Differential Gene Expression in Three Common Rat Models of Diastolic Dysfunction.* Front Cardiovasc Med, 2018. **5**: p. 11.

51. Huang, W., et al., *New Insights into the Tumor Microenvironment Utilizing Protein Array Technology.* Int J Mol Sci, 2018. **19**(2).

52. Luck, C., et al., *Differential Regulation of Cardiac Function and Intracardiac Cytokines by Rapamycin in Healthy and Diabetic Rats.* Oxid Med Cell Longev, 2017. **2017**: p. 5724046.

53. Norum, H.M., et al., *Increased Serum Levels of the Notch Ligand DLL1 are Associated with Diastolic Dysfunction, Reduced Exercise Capacity, and Adverse Outcome in Chronic Heart Failure.* J Card Fail, 2016. **22**(3): p. 218-23.

54. Abad, M., et al., *Notch Inhibition Enhances Cardiac Reprogramming by Increasing MEF2C Transcriptional Activity.* Stem Cell Reports, 2017. **8**(3): p. 548-560.

55. Levick, S.P. and P.H. Goldspink, *Could interferon-gamma be a therapeutic target for treating heart failure?* Heart Fail Rev, 2014. **19**(2): p. 227-36.

56. Kimura, A., et al., *Protective Roles of Interferon-gamma in Cardiac Hypertrophy Induced by Sustained Pressure Overload.* J Am Heart Assoc, 2018. **7**(6).

57. Jin, H., et al., *Inhibitory effects of interferon-gamma on myocardial hypertrophy.* Cytokine, 2005. **31**(6): p. 405-14.

58. Yu, Q., K. Horak, and D.F. Larson, *Role of T lymphocytes in hypertension-induced cardiac extracellular matrix remodeling.* Hypertension, 2006. **48**(1): p. 98-104.

59. Peng, H., et al., *Angiotensin II-induced dilated cardiomyopathy in Balb/c but not C57BL/6J mice.* Exp Physiol, 2011. **96**(8): p. 756-64.

60. Garcia, A.G., et al., *Interferon-gamma ablation exacerbates myocardial hypertrophy in diastolic heart failure.* Am J Physiol Heart Circ Physiol, 2012. **303**(5): p. H587-96.

61. Shintani, Y., et al., *IL-4 as a Repurposed Biological Drug for Myocardial Infarction through Augmentation of Reparative Cardiac Macrophages: Proof-of-Concept Data in Mice.* Sci Rep, 2017. **7**(1): p. 6877.

62. Daseke, M.J., 2nd, et al., *Exogenous IL-4 shuts off pro-inflammation in neutrophils while stimulating anti-inflammation in macrophages to induce neutrophil phagocytosis following myocardial infarction.* J Mol Cell Cardiol, 2020. **145**: p. 112-121.

63. Chang, T.T. and J.W. Chen, *Emerging role of chemokine CC motif ligand 4 related mechanisms in diabetes mellitus and cardiovascular disease: friends or foes?* Cardiovasc Diabetol, 2016. **15**(1): p. 117.

64. Ghanim, H., et al., *Suppressive effect of insulin infusion on chemokines and chemokine receptors.* Diabetes Care, 2010. **33**(5): p. 1103-8.

65. D'Elia, E., et al., *Neprilysin inhibition in heart failure: mechanisms and substrates beyond modulating natriuretic peptides.* Eur J Heart Fail, 2017. **19**(6): p. 710-717.

66. Udelson, J.E., et al., *Rationale and design for a multicenter, randomized, double-blind, placebo-controlled, phase 2 study evaluating the safety and efficacy of the soluble guanylate cyclase stimulator praliciguat over 12 weeks in patients with heart failure with preserved ejection fraction (CAPACITY HFpEF).* Am Heart J, 2020. **222**: p. 183-190.

67. Kovacs, A., et al., *Is enhancing cGMP-PKG signalling a promising therapeutic target for heart failure with preserved ejection fraction?* Neth Heart J, 2016. **24**(4): p. 268-74.

68. Kovacs, A., et al., *Renin overexpression leads to increased titin-based stiffness contributing to diastolic dysfunction in hypertensive mRen2 rats.* Am J Physiol Heart Circ Physiol, 2016. **310**(11): p. H1671-82.

69. Habibi, J., et al., *Mineralocorticoid receptor blockade improves diastolic function independent of blood pressure reduction in a transgenic model of RAAS overexpression.* Am J Physiol Heart Circ Physiol, 2011. **300**(4): p. H1484-91.

70. Heinzel, F.R., et al., *Myocardial hypertrophy and its role in heart failure with preserved ejection fraction.* J Appl Physiol (1985), 2015. **119**(10): p. 1233-42.

71. Karagodin, I., et al., *Echocardiographic evaluation of the effects of sacubitril-valsartan on vascular properties in heart failure patients.* Int J Cardiovasc Imaging, 2020. **36**(2): p. 271-278.

72. Wojtowicz, J., et al., *Central aortic pressure, arterial stiffness and echocardiographic parameters of children with overweight/obesity and arterial hypertension.* Adv Clin Exp Med, 2017. **26**(9): p. 1399-1404.

73. Rees, E., et al., *Central arterial stiffness and diastolic dysfunction are associated with insulin resistance and abdominal obesity in young women but polycystic ovary syndrome does not confer additional risk.* Hum Reprod, 2014. **29**(9): p. 2041-9.

74. Ushiyama, M., T. Kuramochi, and S. Katayama, *Treatment with hypotensive agents affects the impaired relaxation of the penile corpus cavernosum in hypertensive rats.* Hypertens Res, 2006. **29**(7): p. 523-32.

Figure Legends

Figure 1. Ambulatory blood pressure was monitored periodically utilizing radio-telemetric transmitters. Systolic blood pressure (SBP) and diastolic blood pressure were recorded prior to the beginning of treatment and after 3, 5, 7 and 9 weeks of treatment during the light and dark cycles. SBP and DBP increased throughout the course of treatment in ZOC. After 9 weeks of treatment SBP and DBP were significantly reduced in ZOSV during the light and dark periods compared to ZOC ($p<0.05$ indicated by the dagger (†) symbol). N= 4, 4, 3 and 4 for ZOC, ZOSV, ZOV and ZOH, respectively.

Figure 2. Sacubitril/valsartan (sac/val) reduces left ventricular myocardial **a** interstitial and **b** periarterial fibrosis in ZO rats. Representative PSR stained images show fibrosis in the myocardial interstitium in panel **a** or surrounding an arteriole in panel **b**. Accompanying bar graphs show quantitative analysis of average intensity of PSR staining in panel **a** and area of fibrosis normalized to arteriole diameter in panel **b**. Data are represented by means ± SE. n= 5-7 rats per group. Symbols: * indicates $p< 0.05$ versus ZLC; † indicates $p< 0.05$ versus ZOC. Scale bars = 50 μm.

Figure 3. Sacubitril/valsartan (sac/val) reduces myocardial **a** interstitial and **b** periarterial nitroso-oxidative stress in ZO rats. Representative images of 3-nitrotyrosine immunostaining as a marker for nitroso-oxidative stress with accompanying bar graphs showing quantitation of measures of intensity. Data are represented by means ± SE. n=5-7 rats per group. Symbols: * indicates $p< 0.05$ versus ZLC; † indicates $p< 0.05$ versus ZOC.

Figure 4. Sacubitril/valsartan (sac/val) ameliorates in vivo aortic stiffening, as well as endothelial stiffening in ex vivo aortic explants. **a** Pulse wave velocity (PWV) measured after 10 weeks of treatment. **b** Force measurements were acquired by interaction between a cantilever tip and the EC surface of aortic explants from rats after 10 weeks of treatment. **c** Sac/val (▼) and val (△) treatments

prevent impaired responses to the nitric oxide dependent vasodilator, acetylcholine in aortic rings of ZO rats (○). Note the normal reactivity of in ZLC aortae (●). Data are represented by means ± SE in the accompanying bar graph. n= 6-7 rats per group. Symbols: * indicates $p< 0.05$ versus ZLC; † indicates $p< 0.05$ versus ZOC; indicates § $p<0.05$ versus ZOH.

Figure 5. Heatmap illustrating differential cytokine expression in ZOC, ZOV and ZOSV rat cardiac lysates. Individual samples are shown on the x-axis. The y-axis shows statistically significant ($P \leq 0.05$), differentially expressed cytokine markers among the three groups. Each row in the heatmap represents relative changes in the normalized protein expression in the control and treated rats.

Figure 6. Network created by Ingenuity Pathway Analysis from the ZOSV rats. The network was generated from differentially expressed proteins when compared to ZOC rats. The list was selected based on the proteins meeting the threshold of $\log_2$FC of 1.2 and p-value ≤ 0.05. Colored nodes represent the genes derived from our uploaded protein list (focus genes) with green nodes representing downregulation and red nodes representing upregulation. White nodes represent genes or molecules that could potentially be connected to the focus genes and are derived from the IPA knowledge base. The solid lines represent direct interactions between the nodes. A detailed explanation of the molecule shapes is available at http://qiagen.force.com/KnowledgeBase/articles/Basic_Technical_Q_A/Legend.

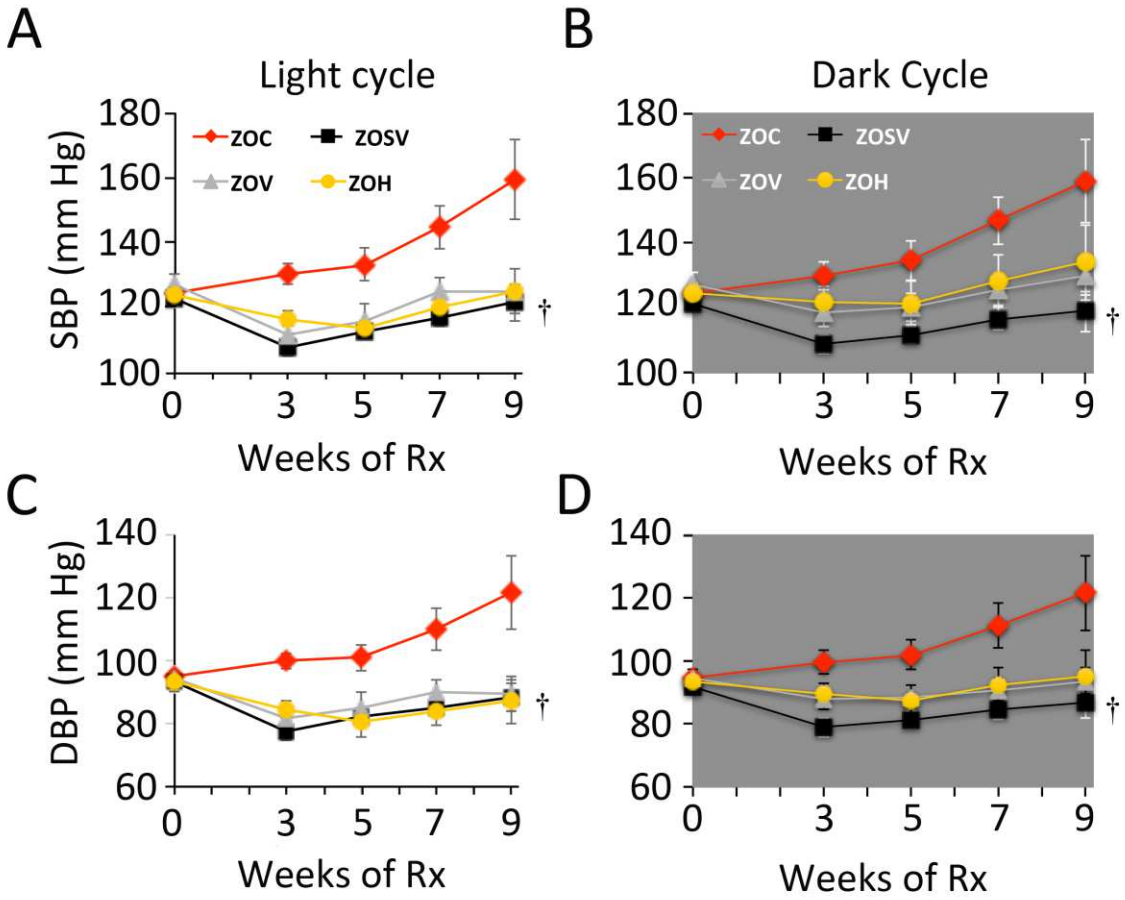
A
Light cycle
SBP (mm Hg)
180
160
140
120
100
ZOC
ZOSV
ZOV
ZOH
0
3
5
7
9
Weeks of Rx
†
B
Dark Cycle
ZOC
ZOSV
ZOV
ZOH
Weeks of Rx
†
C
DBP (mm Hg)
140
120
100
80
60
Weeks of Rx
†
D
Weeks of Rx
†

Figure 1

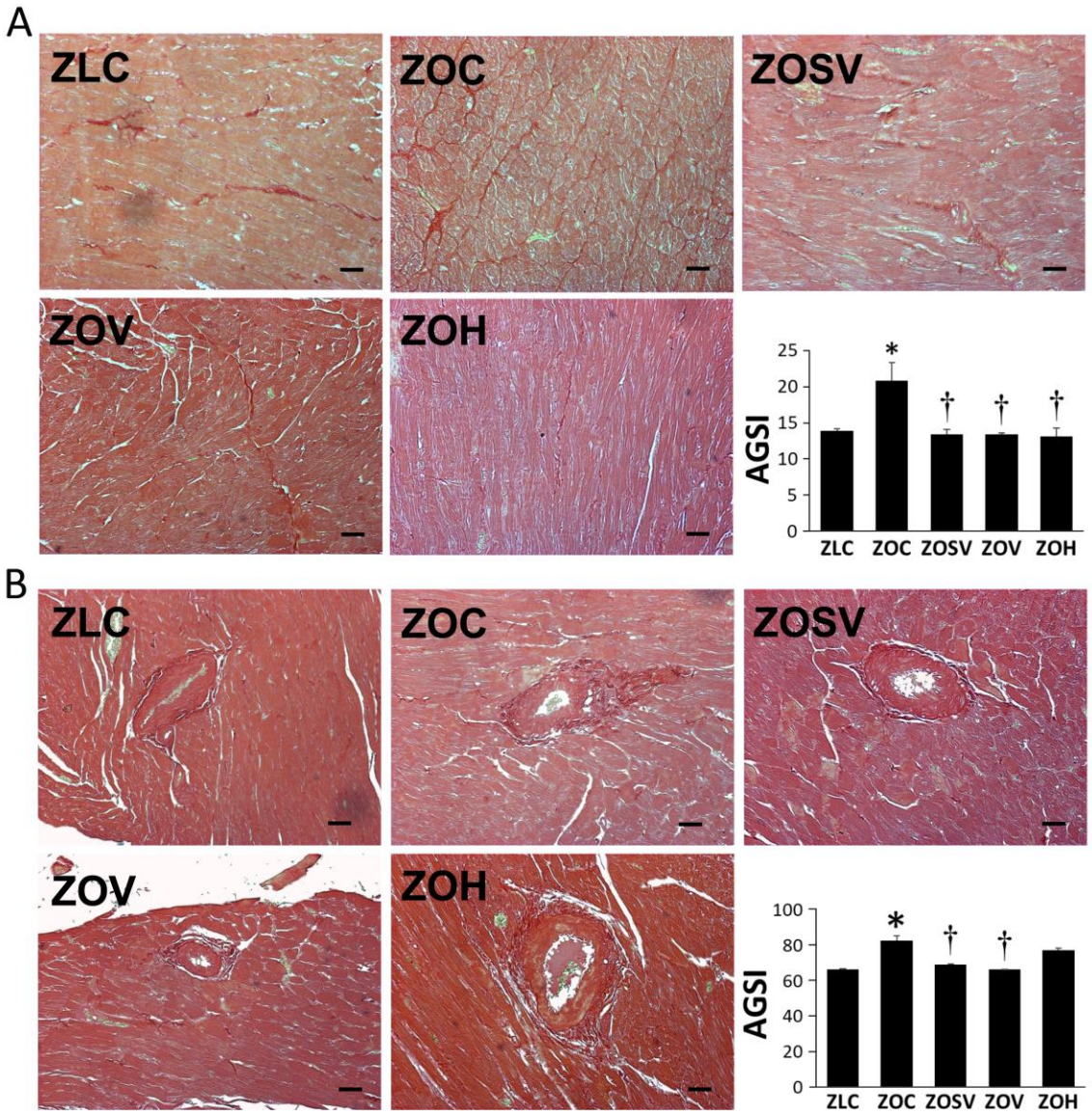
A
ZLC
ZOC
ZOSV
ZOV
ZOH
AGSI
25
20
15
10
5
0
*
†
†
†
ZLC ZOC ZOSV ZOV ZOH
B
ZLC
ZOC
ZOSV
ZOV
ZOH
AGSI
100
80
60
40
20
0
*
†
†
ZLC ZOC ZOSV ZOV ZOH

Figure 2

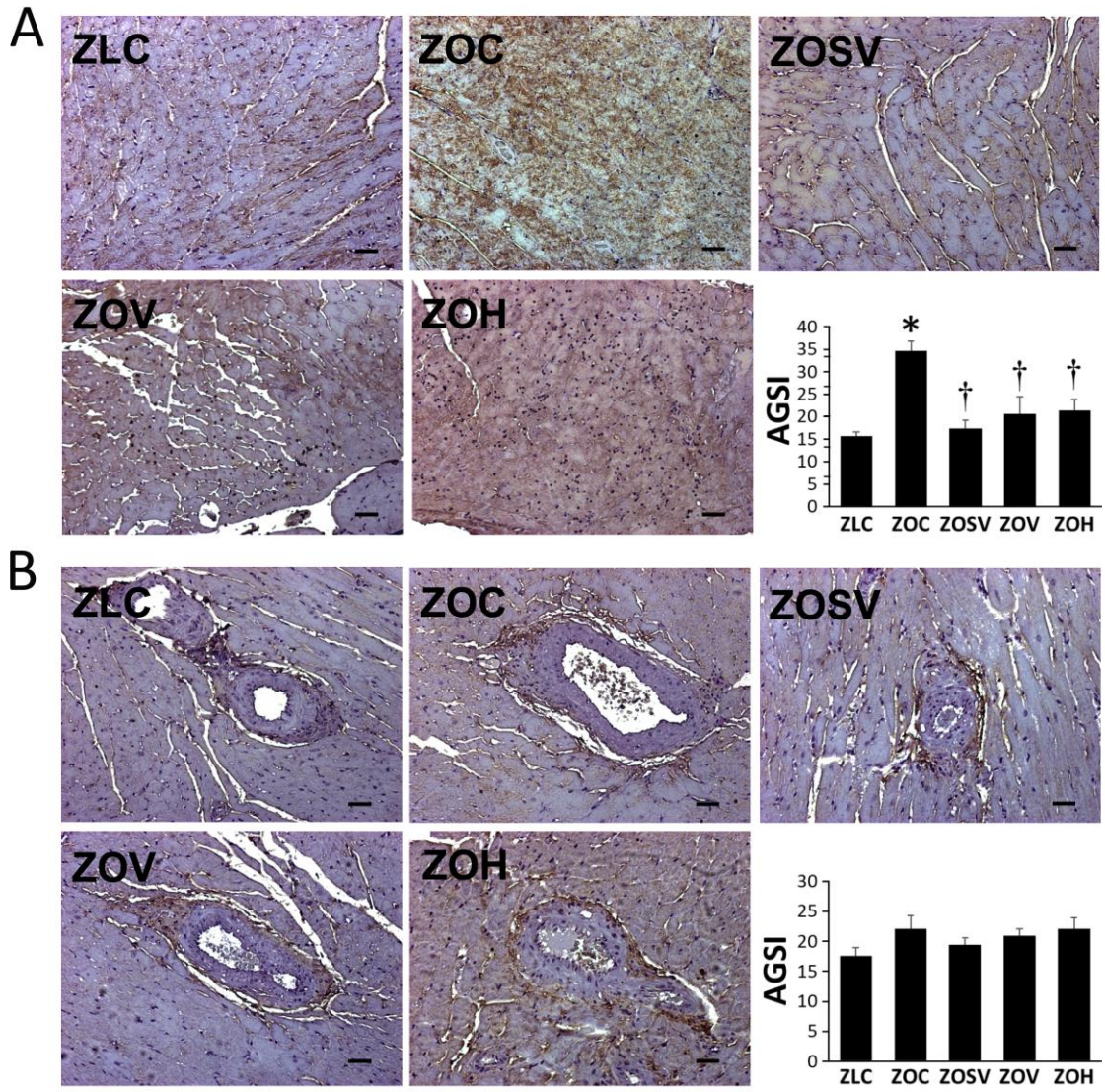
A
ZLC
ZOC
ZOSV
ZOV
ZOH
AGSI
40
35
30
25
20
15
10
5
0
*
†
†
†
ZLC ZOC ZOSV ZOV ZOH
B
ZLC
ZOC
ZOSV
ZOV
ZOH
AGSI
30
25
20
15
10
5
0
ZLC ZOC ZOSV ZOV ZOH

Figure 3

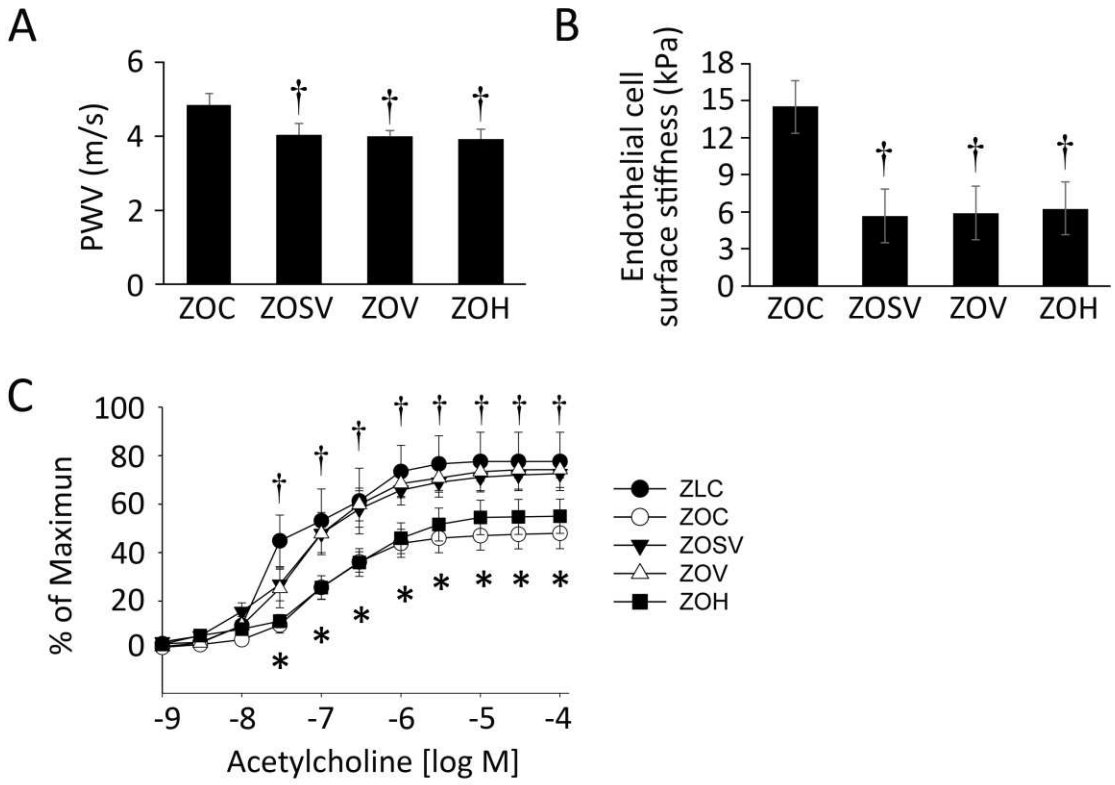
A
PWV (m/s)
6
4
2
0
ZOC ZOSV ZOV ZOH
B
Endothelial cell surface stiffness (kPa)
18
15
12
9
6
3
0
ZOC ZOSV ZOV ZOH
C
% of Maximun
100
80
60
40
20
0
-9 -8 -7 -6 -5 -4
Acetylcholine [log M]
ZLC
ZOC
ZOSV
ZOV
ZOH

Figure 4

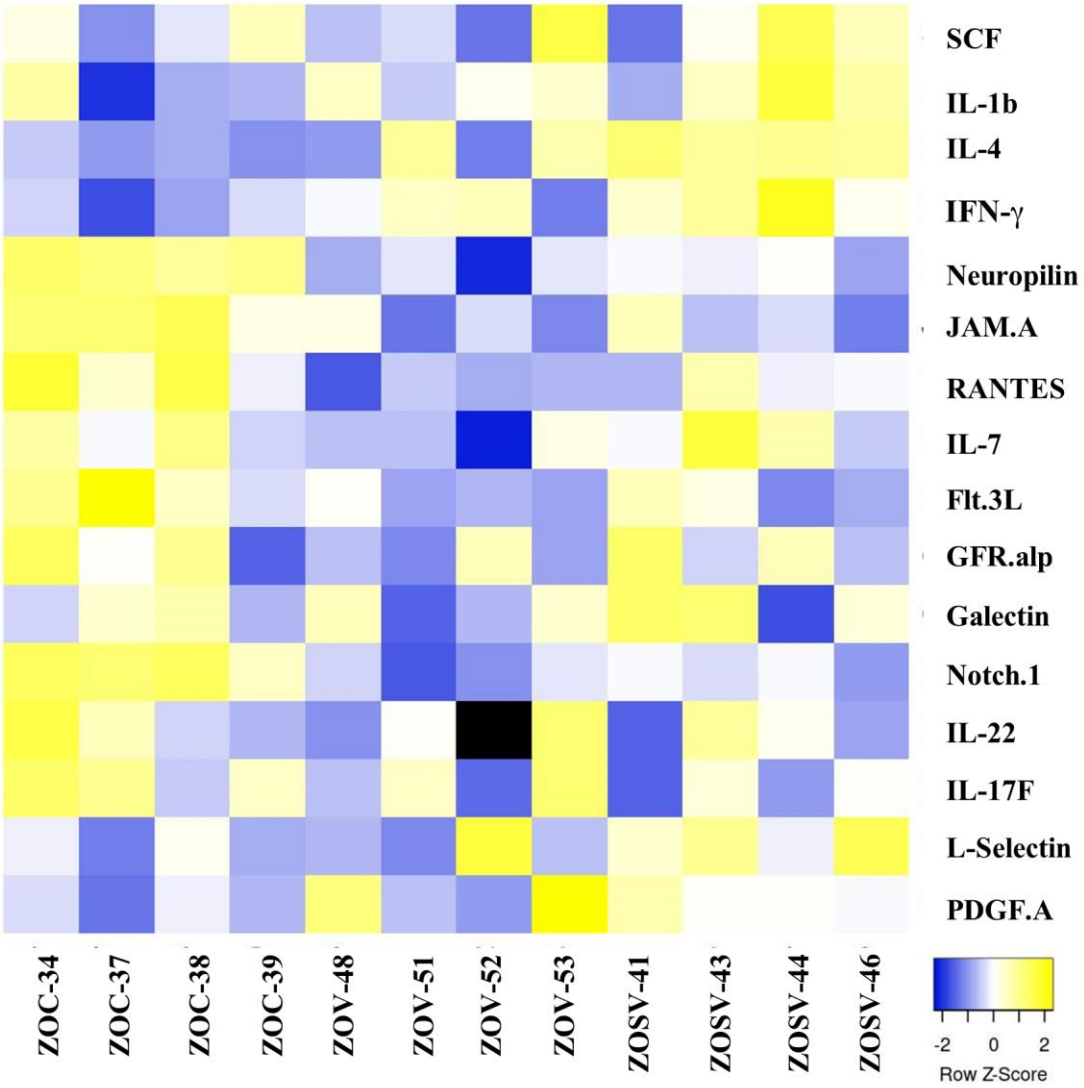
SCF
IL-1b
IL-4
IFN-γ
Neuropilin
JAM.A
RANTES
IL-7
Flt.3L
GFR.alp
Galectin
Notch.1
IL-22
IL-17F
L-Selectin
PDGF.A
ZOC-34
ZOC-37
ZOC-38
ZOC-39
ZOV-48
ZOV-51
ZOV-52
ZOV-53
ZOSV-41
ZOSV-43
ZOSV-44
ZOSV-46
-2
0
2
Row Z-Score

Figure 5.

Figure 6.

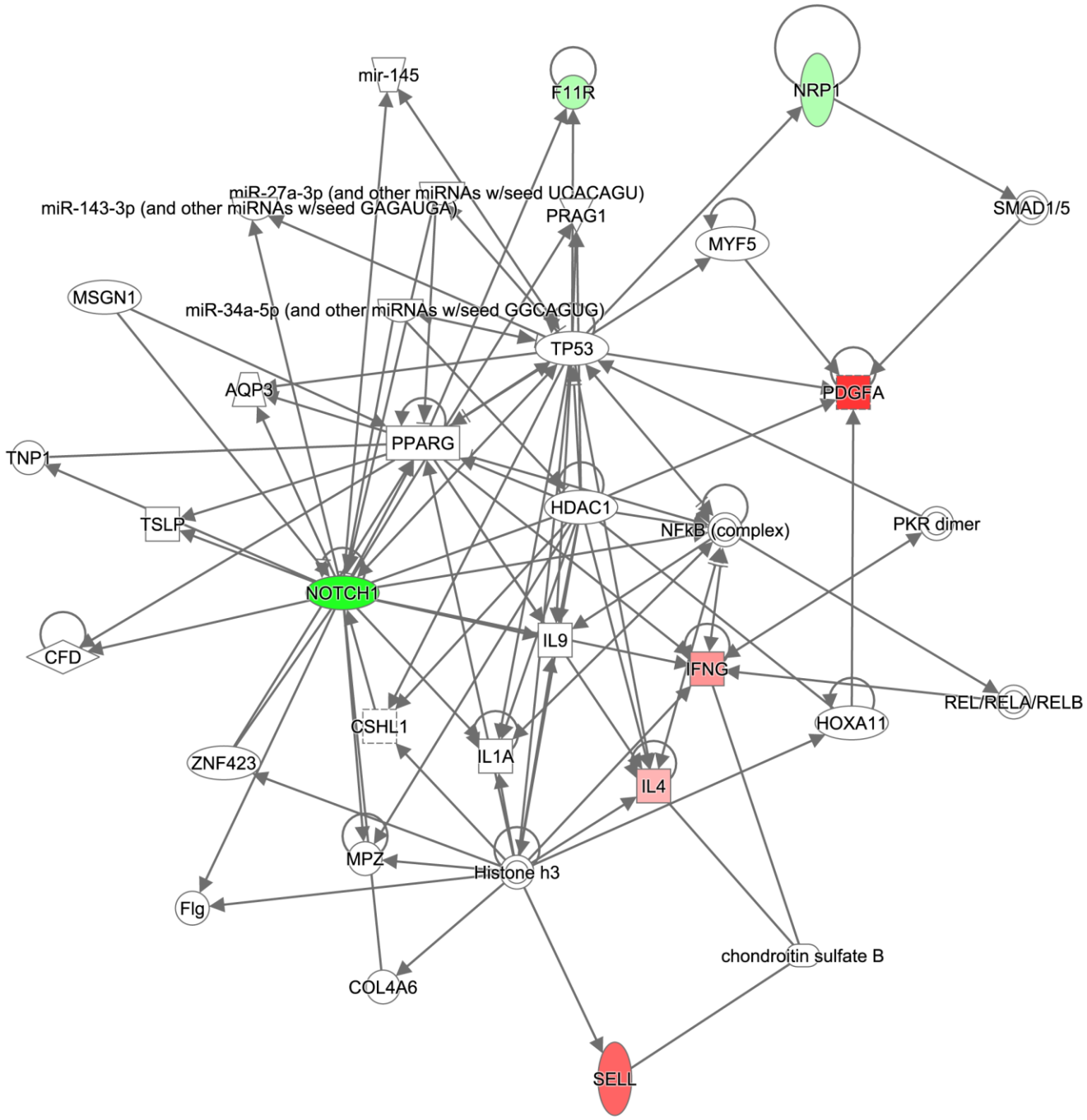
mir-145
F11R
NRP1
miR-27a-3p (and other miRNAs w/seed UCACAGU)
miR-143-3p (and other miRNAs w/seed GAGAUGA)
PRAG1
SMAD1/5
MYF5
MSGN1
miR-34a-5p (and other miRNAs w/seed GGCAGUG)
TP53
AQP3
PDGFA
PPARG
TNP1
HDAC1
TSLP
NFkB (complex)
PKR dimer
NOTCH1
IL9
CFD
IFNG
REL/RELA/RELB
HOXA11
CSHL1
IL1A
ZNF423
IL4
MPZ
Histone h3
Flg
chondroitin sulfate B
COL4A6
SELL

Table 1. Ultrasound derived cardiac function and structure parameters of Zucker Obese rats prior to the ten-week treatment period ($ZOC_{/pre}$) and following the ten week treatment period ($ZOC_{/post}$).

Parameter	$ZOC_{/pre}$ (8-10)	$ZOC_{/post}$ (6-10)
Body Weight (g)	560±7	752±17*
Heart Weight (mg)	NA	1429±62
HW/TL ($mg \bullet mm^{-1}$)	NA	18.1±0.5
systolic parameters		
Ejection Fraction (%)	82±2	76±2*
Cardiac Output ($ml \bullet min^{-1}$)	302±56	270±29
Stroke Volume (µl)	828±164	762±90
IVCT (ms)	12.5±0.9	15.5±0.6
s' ($mm \bullet sec^{-1}$)	43±1	42±3
Ejection Time (ms)	65±3	71±2
LVETI	695±22	685±17
Systolic Time (ms)	99±3	112±3*
diastolic parameters		
E, ($mm \bullet sec^{-1}$)	921±49	1117±126
A, ($mm \bullet sec^{-1}$) late	828±60	1036±127
E/A ratio	1.06±0.05	1.07±0.08
e', ($mm \bullet sec^{-1}$)	36±2	52±6*
a', ($mm \bullet sec^{-1}$)	54±5	69±10
e'/a' ratio	0.69±0.06	0.76±0.05
E/e' (LV filling pressure)	24.5±1.0	22.7±2.6
Diastolic Stiffness (E/e'/LVIDd)	3.26±0.10	2.68±0.29
IVRT (ms)	20.8±0.9	25.8±1.4*
MPI	0.54±0.04	0.58±0.01
structural parameters		
LA/Ao ratio	1.51±0.06	1.38±0.11
LV Mass (mg)	926±44	1067±19*
AWTd (mm)	2.12±0.09	2.07±0.05
PWTd (mm)	1.87±0.09	1.83±0.11
Relative Wall Thickness	0.53±0.03	0.46±0.03
LVIDd (mm)	7.55±0.11	8.45±0.21*
LVIDs (mm)	3.60±0.16	4.44±0.16*

Values are mean ± SE, n=6-10 (sample sizes shown in parentheses). *$p<0.05$ vs $ZOC_{/pre}$. Heart weight=HW; tibia length=tibia length; LV=left ventricle; e'=early septal wall velocity during diastole; a'= late septal wall velocity during diastole; s'=peak septal wall velocity during systole; E=early mitral flow velocity; A=late mitral flow velocity; E/E'=LV filling pressure; IVRT=isovolumic relaxation time; IVCT=isovolumic contraction time; MPI=myocardial performance index; LVETI=LV ejection time index; LA=left atrium diameter; Ao=aorta diameter; AWTd=anterior wall thickness at end

diastole; PWTd=posterior wall thickness at end diastole; LVIDd=LV inner diameter at end diastole; LVIDs=LV inner diameter at end systole.

Table 2. Ultrasound derived cardiac function and structure parameters of lean and obese Zucker rats.

Parameter	ZLC (3-6)	ZOC (6-10)	ZOSV (6-11)	ZOV (6-11)	ZOH (6-11)
Heart Weight (mg)	1147±41	1429±62*	1392±67*§	1302±35*§	1639±50*
HW/TL (mg●mm^{-1})	10.5±0.3	18.1±0.5*	16.8±0.7*§	17.3±0.4§	15.8±0.6*
systolic parameters					
Ejection Fraction (%)	69±3	76±2	81±2*	80±2*	80±4*
Cardiac Output (ml●min^{-1})	190±23	270±29	281±24*	260±19§	342±36*
Stroke Volume (µl)	504±52	762±90	828±74*	768±54	874±111*
IVCT (ms)	12.5±0.9	15.5±0.6	11.7±1.3†	13.7±1.9	13.5±2.9
s' (mm●sec^{-1})	58±1	42±3*	41±1*	43±3*	48±6
diastolic parameters					
E, (mm●sec^{-1})	888±56	1117±126	894±53	1095±63	1091±60
A, (mm●sec^{-1}) late	886±36	1036±127	814±70	973±54	1098±127
E/A ratio	1.00±0.04	1.07±0.08	1.12±0.06	1.15±0.11	1.03±0.11
e', (mm●sec^{-1})	94±7	52±6*	55±7*	56±8*	76±10
a', (mm●sec^{-1})	76±4	69±10	51±3*§	76±6‡	68±4‡
e'/a' ratio	1.23±0.03	0.76±0.05*	1.08±0.12†	0.75±0.08*‡§	1.12±0.13†
E/e' (LV filling pressure)	10.3±0.7	22.7±2.6*	17.1±1.5	20.9±2.4*	15.5±2.6
Diastolic Stiffness (E/e'/LVIDd)	1.16±0.13	2.68±0.29*	2.09±0.22*	2.51±0.30*§	1.67±0.25†
IVRT (ms)	17.5±0.7	25.8±1.4*	21.3±0.7*†	20.3±0.6*†	18.4±1.8†
Ejection Time (ms)	64.7±2.4	71.1±1.7	68.4±1.8	66.5±3.1	60.4±2.0
LVETI	702±13	685±17	650±12*	716±32	679±27
MPI	0.47±0.03	0.58±0.01*	0.49±0.03†	0.52±0.04	0.52±0.06
structural parameters					
LA/Ao ratio	0.95±0.05	1.38±0.11*	1.23±0.10*	1.28±0.03*	1.35±0.05*
LV Mass (mg)	863±35	1067±19*	1104±73*§	976±45§	1340±64*†
AWTd (mm)	1.60±0.07	2.07±0.05*	2.07±0.16*	1.87±0.07	2.03±0.08*
PWTd (mm)	1.68±0.06	1.83±0.11	2.04±0.16*	1.81±0.10	2.08±0.05*
Relative Wall Thickness	0.38±0.02	0.46±0.03*	0.50±0.04*	0.44±0.02*	0.45±0.02*
LVIDd (mm)	8.71±0.25	8.45±0.21	8.26±0.17§	8.32±0.14§	9.22±0.26†
LVIDs (mm)	5.24±0.29	4.44±0.16*	3.99±0.26*	4.09±0.23*	4.55±0.47

Values are mean ± SE, n=6-11 (sample sizes shown in parentheses). *p<0.05 vs ZLC; †p<0.05 vs ZOC; §p<0.05 vs ZOH; ‡p<0.05 vs ZOL; [a]p<0.06 vs ZLC; [b]p<0.07 vs ZLC. Heart weight=HW; tibia length=tibia length; LV=left ventricle; e'=early septal wall velocity during diastole; a'= late septal wall velocity during diastole; s'=peak septal wall velocity during systole; E=early mitral flow velocity; A=late mitral flow velocity; E/E'=LV filling pressure; IVRT=isovolumic relaxation time; IVCT=isovolumic contraction time; MPI=myocardial performance index; LVETI=LV ejection time index; LA=left atrium diameter; Ao=aorta diameter; AWTd=anterior wall thickness at end diastole; PWTd=posterior wall thickness at end diastole; LVIDd=LV inner diameter at end diastole; LVIDs=LV inner diameter at end systole.

Table 3. Summary of cytokine profile changes in Zucker Obese (ZOC) rats when compared to control rats (ZLC). Molecules on the cytokine array that showed at least log_2 fold-change (log_2FC) of 1.2 and with a p-value ≤ 0.05 are shown. Statistical significance between the indicated groups determined by unpaired two-tailed t-tests. Gene symbols corresponding to each cytokine are shown.

Molecule	Gene	ZOC/ZLC	
		log_2FC	P-value
RANTES	*Ccl5*	-1.288	0.050
PDGF-AA	*Pdgfa*	-1.359	0.012
GFR alpha-1	*Gfra1*	-0.885	0.049
SCF	*Kitl*	-0.269	0.043
IL-7	*Il7*	-0.655	0.024

RANTES, Regulated upon Activation, Normal T Cell Expressed and Presumably Secreted; PDGF, Platelet Derived Growth Factor; GFR alpha 1, Glial Cell line-derived Neurotrophic Factor Receptor Alpha 1; SCF, Stem Cell Factor; IL, Interleukin

Table 4. Summary of cytokine profile changes in Zucker Obese (ZO) rats treated with sacubitril/valsartan (ZOSV), valsartan (ZOV), and hydralazine (ZOH) when compared to control rats (ZOC). Molecules on the cytokine array that showed at least $\log_2$ fold-change ($\log_2$FC) of 1.2 and with a p-value ≤ 0.05 are shown. Statistical significance between the indicated groups determined by unpaired two-tailed t-tests. Gene symbols corresponding to each cytokine are shown.

Molecule	Gene	ZOSV /ZOC		ZOV/ZOC		ZOH/ZOC	
		$\log_2$FC	P-value	$\log_2$FC	P-value	$\log_2$FC	P-value
Neuropilin-1	*Nrp1*	-0.266	0.001	-0.398	0.005	-0.173	0.052
Notch-1	*Notch1*	-0.768	0.003	-1.108	0.002	-0.976	0.002
PDGF-AA	*Pdgfa*	1.054	0.041				
L-Selectin	*Sell*	0.800	0.044				
IFNg	*Ifng*	0.550	0.020				
IL-4	*Il4*	0.386	2.61E-05				
JAM-A	*F11r*	-0.271	0.021	-0.317	0.010		
RANTES	*Ccl5*			-0.436	0.014		
Flt-3L	*Flt3l*			-0.464	0.047		
IL-17F	*Il17f*					-0.668	0.037
Galectin-3	*Lgals3*					-0.572	0.044

Notch, Notch receptor 1; IFN, Interferon; JAM-A, Junctional Adhesion Molecule A; Flt-3L, FMS related Receptor Tyrosine Kinase 3 Ligand.

Figures

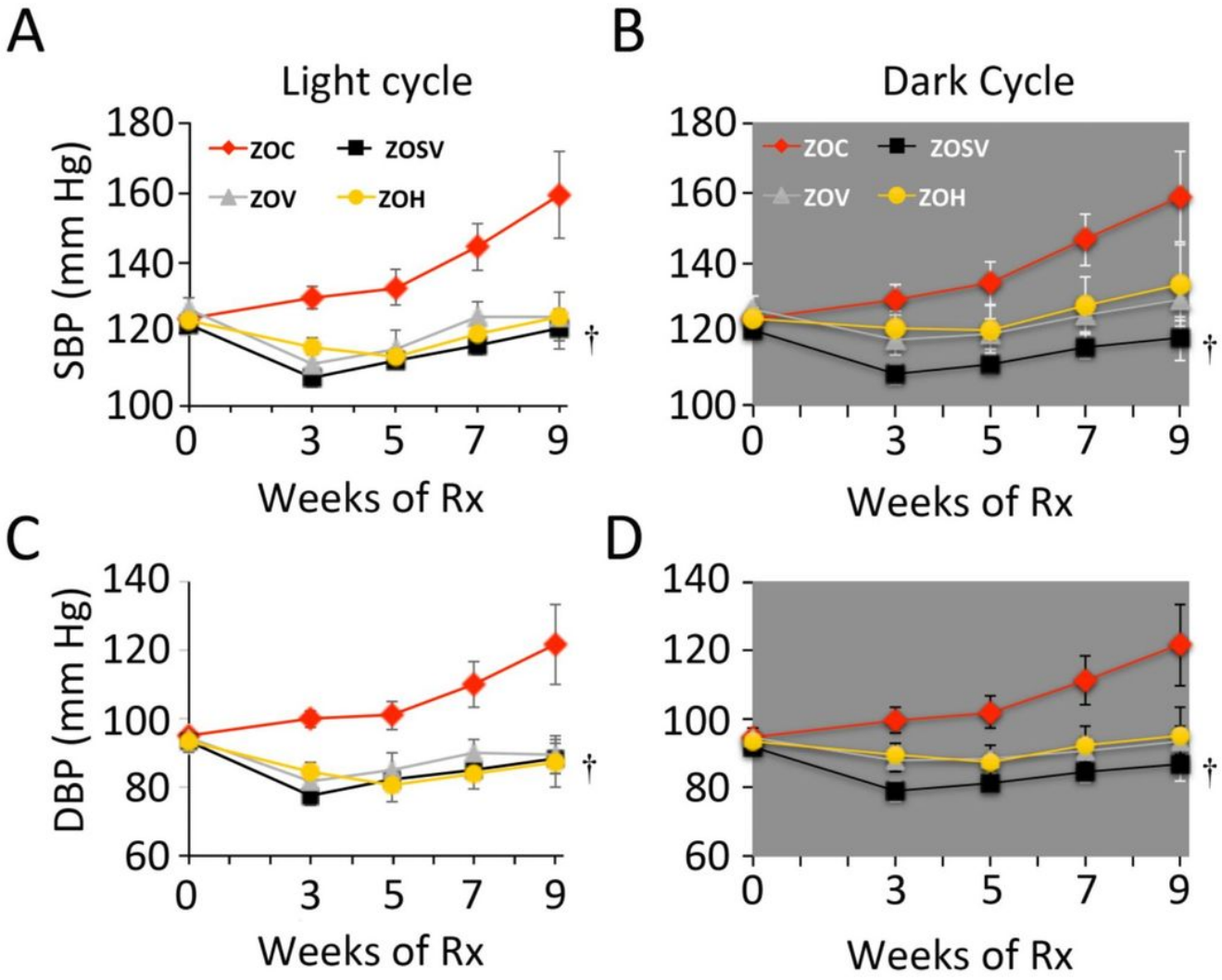

Figure 1

Ambulatory blood pressure was monitored periodically utilizing radio-telemetric transmitters. Systolic blood pressure (SBP) and diastolic blood pressure were recorded prior to the beginning of treatment and after 3, 5, 7 and 9 weeks of treatment during the light and dark cycles. SBP and DBP increased throughout the course of treatment in ZOC. After 9 weeks of treatment SBP and DBP were significantly reduced in ZOSV during the light and dark periods compared to ZOC ($p<0.05$ indicated by the dagger (†) symbol). N= 4, 4, 3 and 4 for ZOC, ZOSV, ZOV and ZOH, respectively.

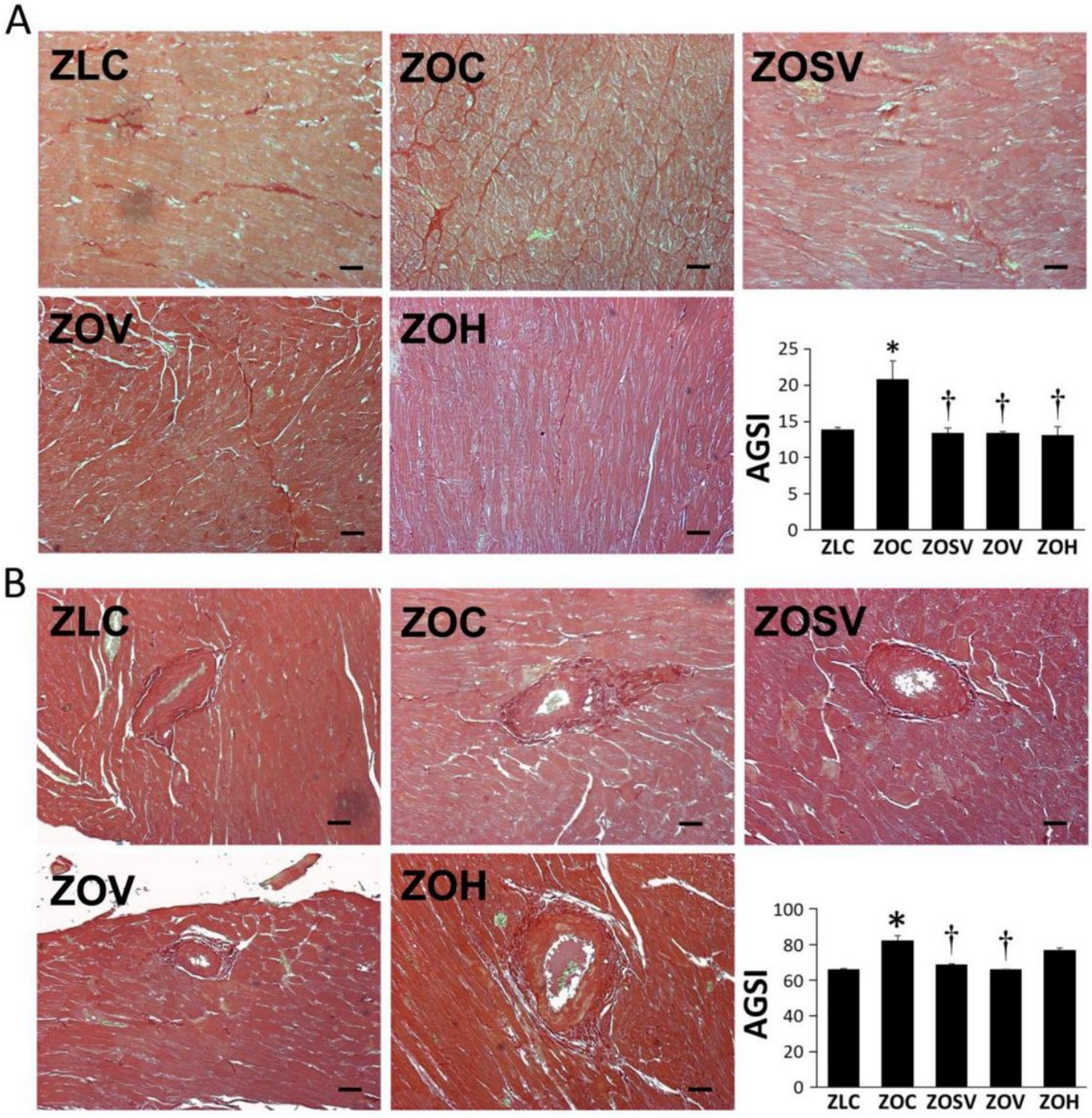

Figure 2

Sacubitril/valsartan (sac/val) reduces left ventricular myocardial a interstitial and b periarterial fibrosis in ZO rats. Representative PSR stained images show fibrosis in the myocardial interstitium in panel a or surrounding an arteriole in panel b. Accompanying bar graphs show quantitative analysis of average intensity of PSR staining in panel a and area of fibrosis normalized to arteriole diameter in panel b. Data are represented by means ± SE. n= 5-7 rats per group. Symbols: * indicates $p< 0.05$ versus ZLC; † indicates $p< 0.05$ versus ZOC. Scale bars = 50 μm.

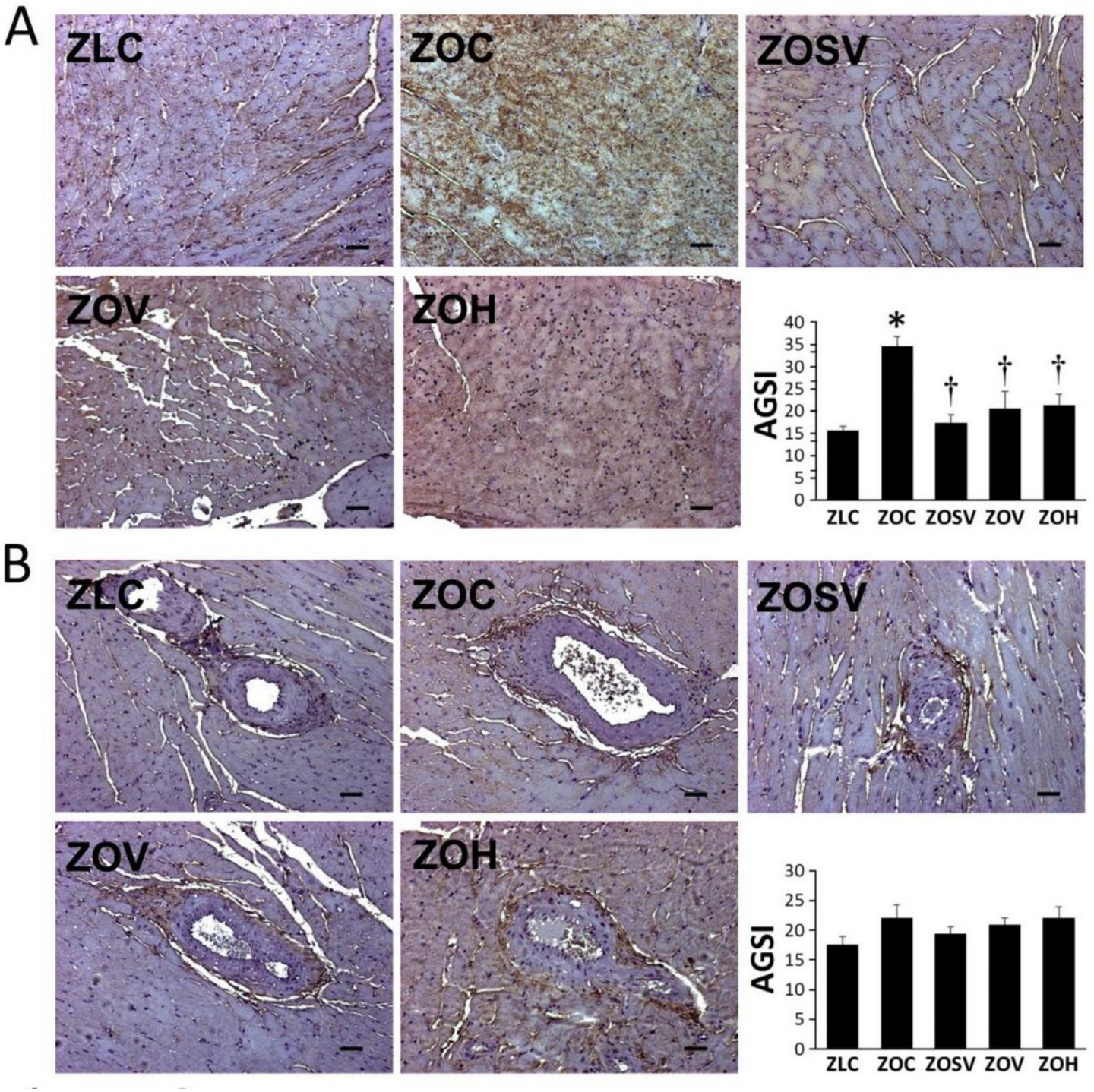

Figure 3

Sacubitril/valsartan (sac/val) reduces myocardial a interstitial and b periarterial nitroso oxidative stress in ZO rats. Representative images of 3-nitrotyrosine immunostaining as a marker for nitroso-oxidative stress with accompanying bar graphs showing quantitation of measures of intensity. Data are represented by means ± SE. n=5-7 rats per group. Symbols: * indicates $p< 0.05$ versus ZLC; † indicates $p< 0.05$ versus ZOC.

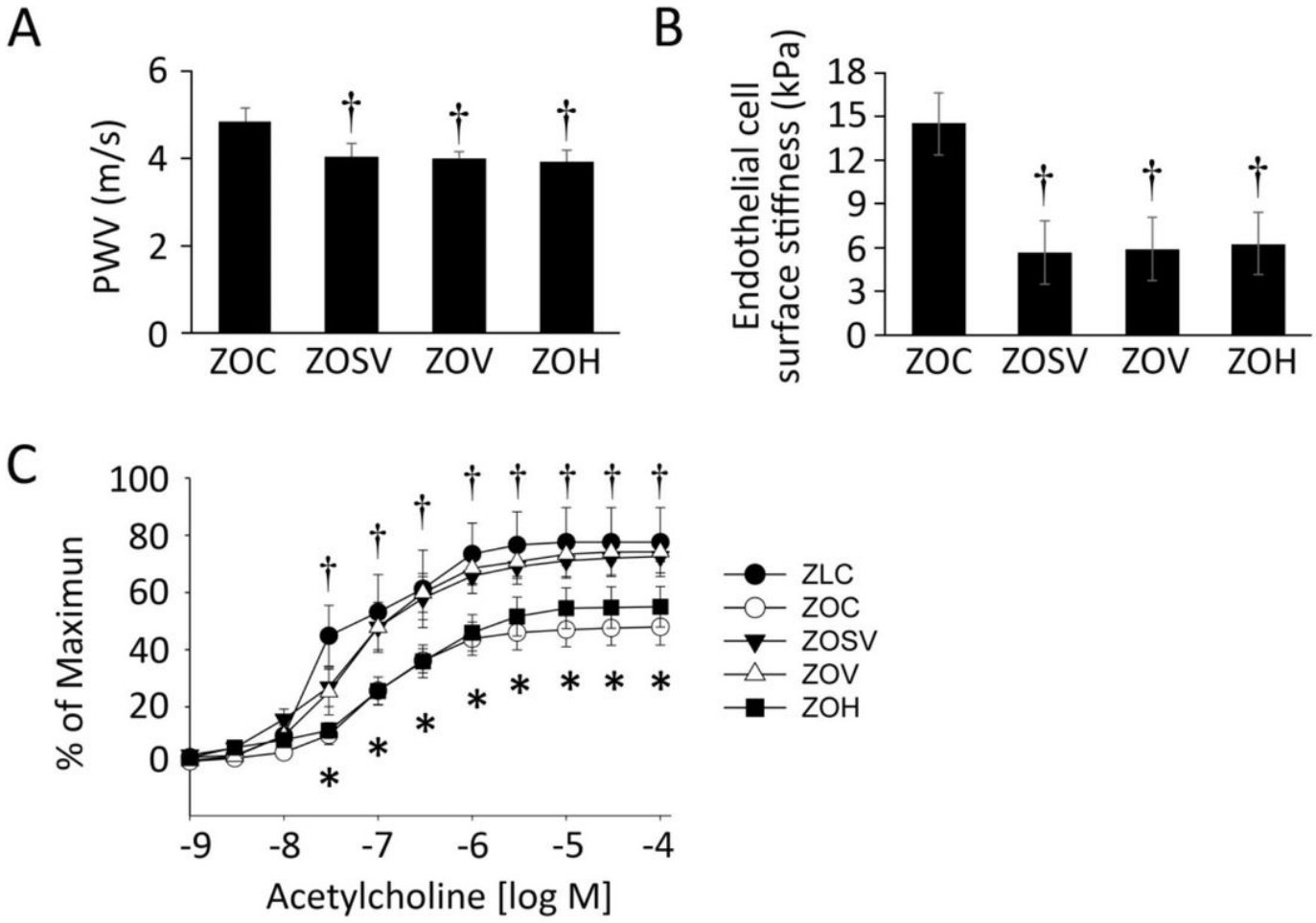

Figure 4

Sacubitril/valsartan (sac/val) ameliorates in vivo aortic stiffening, as well as endothelial stiffening in ex vivo aortic explants. a Pulse wave velocity (PWV) measured after 10 weeks of treatment. b Force measurements were acquired by interaction between a cantilever tip and the EC surface of aortic explants from rats after 10 weeks of treatment. c Sac/val (□) and val (Δ) treatments prevent impaired responses to the nitric oxide dependent vasodilator, acetylcholine in aortic rings of ZO rats (□). Note the normal reactivity of in ZLC aortae (□). Data are represented by means ± SE in the accompanying bar graph. n= 6-7 rats per group. Symbols: * indicates p< 0.05 versus ZLC; † indicates p< 0.05 versus ZOC; indicates § p<0.05 versus ZOH.

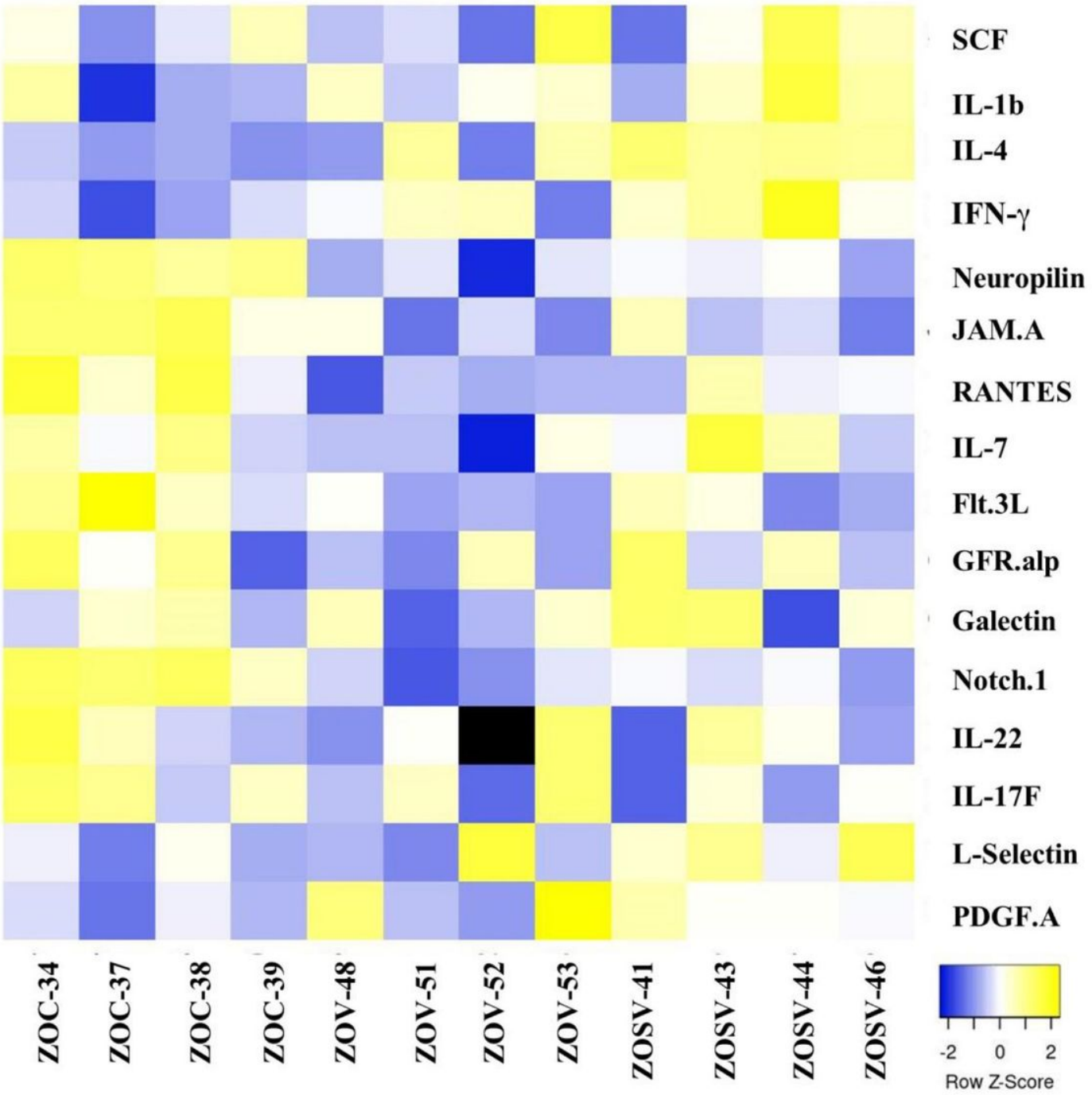

Figure 5

Heatmap illustrating differential cytokine expression in ZOC, ZOV and ZOSV rat cardiac lysates. Individual samples are shown on the x-axis. The y-axis shows statistically significant ($P \leq 0.05$), differentially expressed cytokine markers among the three groups. Each row in the heatmap represents relative changes in the normalized protein expression in the control and treated rats.

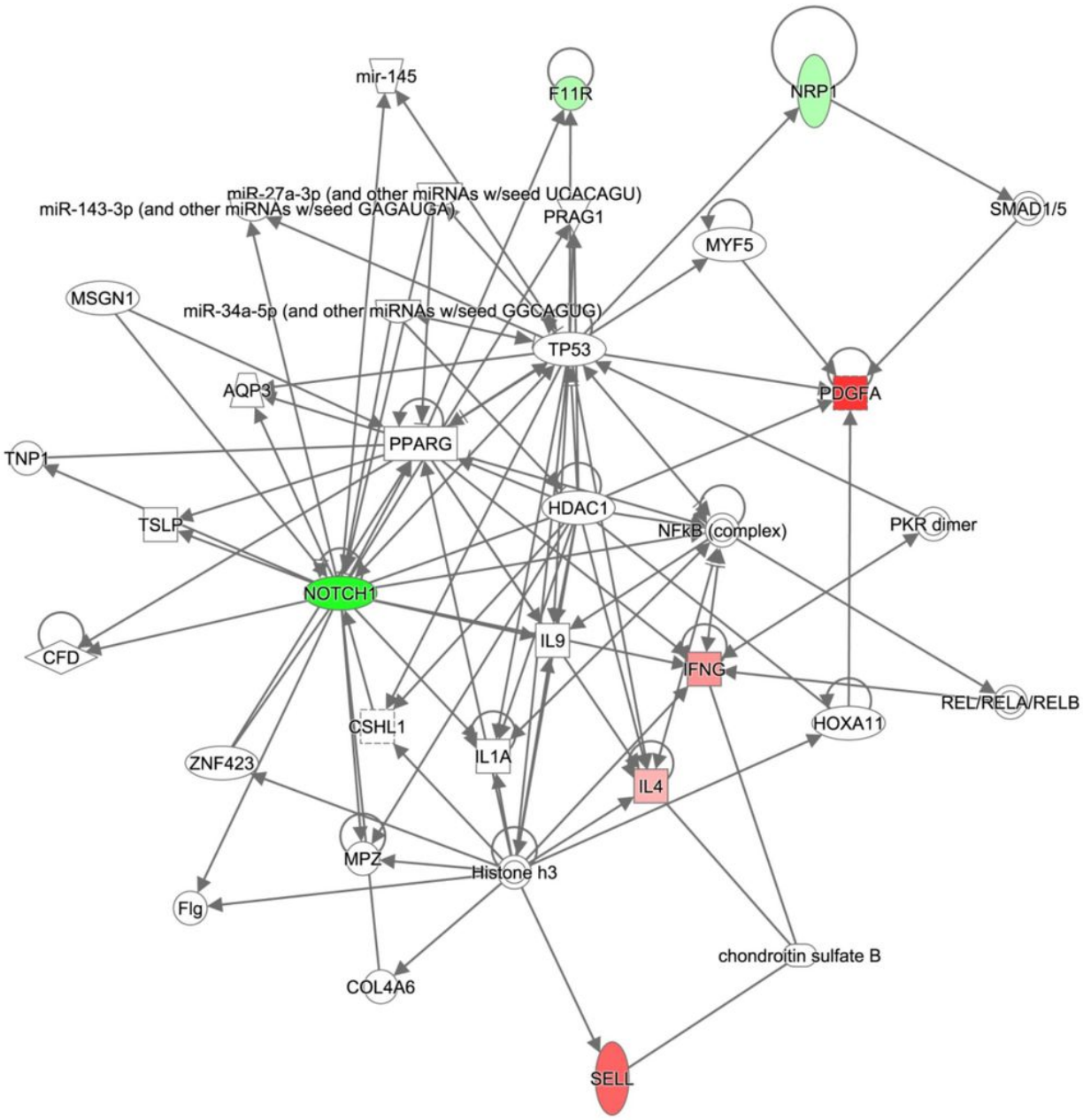

Figure 6

Network created by Ingenuity Pathway Analysis from the ZOSV rats. The network was generated from differentially expressed proteins when compared to ZOC rats. The list was selected based on the proteins meeting the threshold of log2FC of 1.2 and p-value ≤ 0.05. Colored nodes represent the genes derived from our uploaded protein list (focus genes) with green nodes representing downregulation and red nodes representing upregulation. White nodes represent genes or molecules that could potentially be connected to the focus genes and are derived from the IPA knowledge base. The solid lines represent direct interactions between the nodes. A detailed explanation of the molecule shapes is available at http://qiagen.force.com/KnowledgeBase/articles/Basic_Technical_Q_A/Legend.